NUMERICAL MODELLING OF THE COASTAL OCEAN OFF TANZANIA

MAJUTO CLEMENT MANYILIZU

DEPARTMENT OF OCEANOGRAPHY,

UNIVERSITY OF CAPE TOWN.

RONDEBOSCH, SOUTH AFRICA

Dissertation submitted to the faculty of Science, University of Cape Town, in partial fulfillment of the requirements for the Applied Marine Science, Master of Science Degree. 2009.

DECLARATION

This work has not been submitted in whole, or in part, for the award of any degree. It is my own work. Each significant contribution to, and quotation in this dissertation from the work, or works of other people has been attributed, and has been cited and referenced.

Full name: **Majuto Clement Manyilizu**

Signature: Signed by candidate

Date: 25th of May, 2009.

Table of Contents

Abstract

In this model study of the coastal ocean off Tanzania, the Regional Ocean Modelling System (ROMS) was employed to model the coastal ocean off Tanzania over the domain of 5^0N-15^0S and 38-55^0E. It was integrated for ten years with monthly mean Comprehensive Ocean and Atmosphere Data Sets (COADS) winds and heat fluxes. Initial and lateral boundary conditions were derived from the World Ocean Atlas. The model was used to simulate the annual cycle, and the sea surface temperature (SST) output compared with the Tropical Rainfall Measuring Mission (**TRMM**) Microwave Imager (**TMI**) sea surface temperature (SST) measurements for the same region.

Although broadly comparable, the model SST was generally warmer than that of TMI data. The high SSTs in the Tanzanian coastal waters (greater than 28^0C) occur from December to May while SSTs of less than 28^0C occur during the rest of the year. The East African Coastal Current (EACC) experiences its lowest spatial and temporal average speeds (about 0.4ms^{-1}) in February and its maximum speed (1.7 ms^{-1}) in July. Speeds of greater than 1 ms^{-1} occur during both transition seasons north of 6^0S. The meridional wind stresses appear to be positively correlated with the EACC($r>0.6$) in all locations and they are statistically significant ($p<0.05$). The annual cycle of the model flow in the southern Tanzanian waters seems to be positively correlated with the flow to the north of Madagascar ($r=0.57$ and $p=0.05$). The flow in these regions changes in phase with each other from October to April and June to July with minimum speeds in November. For the other months, the flow in these regions is out of phase with each other. The model currents off southern Tanzania

attain their maximum speeds in August when the South West monsoon is fully developed while the flow north of Madagascar attains its maximum speed in September when the South West monsoon fades. However, the flow in the southern Tanzanian waters is more affected by the reversal of winds over the tropical western Indian Ocean ($r=0.69$, $p=0.01$) than that north of Madagascar ($r=0.51$, $p=0.09$). This difference results in a larger annual speed range in the flow off southern Tanzania (about 0.4 ms^{-1}) than that to the north of Madagascar (about 0.3ms^{-1}).

The ROMS model realistically simulates the annual cycle of the sea surface temperature and heat flux, the East African Coastal Current and the annual cycle of the flow entering the coastal ocean off the southern part of Tanzania. However, studies which integrate the large scale domain and regional coupled ocean-atmosphere interactions are needed to better understand of the East African climate and ocean variability. Such model results combined with suitable remote sensing and *in situ* observations will help improve understanding of the circulation and properties of the coastal ocean off Tanzania.

Acknowledgements

I am forever grateful to members of our family; my father Nyelu C. Manyilizu, my mother Kashindye Musili, my brothers and my sisters for their support and sacrifice in my academic career. I love all of them so much and my debt to them is beyond measure.

I express my gratitude to my supervisor Prof. Chris Reason and head of department Prof. Frank Shillington for their guidance, encouragement and assistance during my course. I also thank all students and staff in the Department of Oceanography, University of Cape Town for their cooperation and support during my course.

Special thanks to the Institute of Marine Sciences (IMS), University of Dar es Salaam under the auspices of the Sida-SAREC Bilateral Marine Science Program through its director, Prof. Alfonse Dubi for the financial support and cooperation while I was studying. The skills and knowledge that I have acquired will be beneficial to the Institute of Marine Sciences and Tanzania.

List of figures and tables

Figure 2.8: The Indian Ocean Dipole Zonal Mode (IODZM) index for 1990-2008, with the strongest positive events (index > 0.5℃) and negative events (index < -0.5℃) highlighted in red and blue respectively (After McPhaden et al, 2008)

Figure 3.1: The map of the domain region of the study of the Tanzanian waters. (http://rimmer.ngdc.noaa.gov).

Figure 4.1a-i: The properties of the East African coastal ocean for May (panels a, b and c), July (panels d, e and f), September (panels g, h and i) showing model net surface heat flux in column one, model SST in column two and satellite derived (TMI) SST in column three.

Figure 4.1j-r: The same as figure 4.1a-i but for November (panels j, k and l), January (panels m, n and o) and March (panels p, q and r).

Figure 4.2: COADS wind stress field in Nm^{-2} over the East African coastal ocean for May (a), July (b), September (c), November (d), January (e) and March (f).

Figure 4.3 (a-f): The East African Coastal Current (EACC) speeds (ms^{-1}) from January to June.

Figure 4.3 (g-l): The East African Coastal Current (EACC) speeds (ms^{-1}) from July to December.

Figure 4.4a: Time series of the East African Coastal Current (EACC) speeds (ms^{-1}) and meridional wind stresses (Nm^{-2}). A correlation coefficient r =0.69 and p=0.01 was computed between these two variables at 10^0S and between 40^0 and 42^0E off coast of East Africa.

Figure 4.4b: The same as figure 4.4a at 8^0S but with the correlation coefficient r =0.89 and p=0.001.

Figure 4.4c: The same as figure 4.4a at 6^0S but with the correlation coefficient r =0.74 and p=0.01

Figure 4.4d: The same as figure 4.4a at 4^0S but with the correlation coefficient r =0.70 and p=0.01

Figure 4.4e: The same as figure 4.4a at 2^0S but with the correlation coefficient r =0.64 and p=0.03.

Figure.4.5: The time series of the mean speeds (ms^{-1}) of the EACC and NEMC in the southern Tanzanian coastal ocean (10^0S, 40-42^0E) and the NEMC to the north of Madagascar (11.8^0S, 49^0E) respectively. A correlation coefficient r =0.57 and p=0.05 is computed between these two variables.

Figure 4.6: The time series of the mean speeds (ms^{-1}) of the NEMC and the meridional wind stress (Nm^{-2}) to the north of Madagascar at 11.8^0S and 49^0E. A correlation coefficient r =0.51 and p=0.09 is computed between these two variables.

Table 4.1: The monthly mean speeds (ms^{-1}) of the East African Coastal Current (EACC) derived from the model time series Figures 4.4a-d.

Chapter 1 Introduction

1.1 Introduction

The Indian Ocean is smaller than either the Pacific or Atlantic Ocean. It is blocked in the north at about 25^0N by the Asian landmass and by East Africa to the west. Its wind systems are mainly controlled by the large scale atmospheric systems in both subtropics, the Arabian high (ridge) in the Northern Hemisphere and the Mascarene high located east or south of Madagascar in the Southern Hemisphere. The seasonal variability of the pressure gradient between the Arabian high and Madagascar results in the seasonal reversals in direction of the winds. This leads to the South West monsoon during austral winter and the North East monsoon during austral summer. During austral summer, a pressure gradient of about 6hPa is created between Arabia and Madagascar resulting in the North East monsoon. In austral winter, the pressure gradient from Madagascar to Arabia reaches about 22hPa due to the strong heating of the Asian landmass. As a result, the winds blowing towards Asian landmass (the South West monsoon) are much stronger than the North East monsoon. The monsoonal winds are influenced by the Coriolis effects and by regional topography (e.g., East African highlands) so that they blow along a southwest to northeast direction rather than south to north. This monsoon system affects the Indian Ocean circulation throughout the year as shown in figure 1.1.

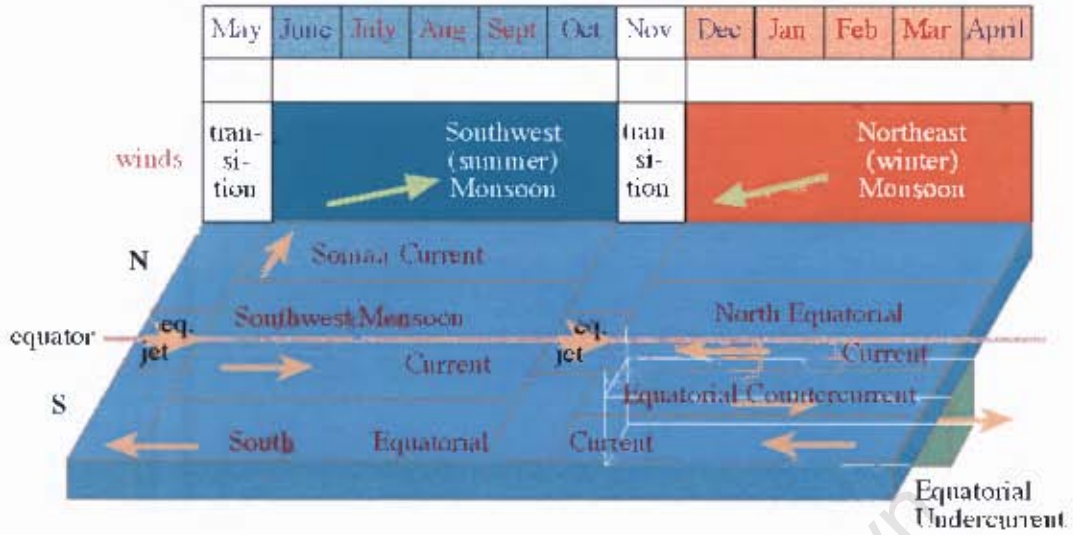

Figure1.1: The monthly wind flow cycles (top) and response of the Indian Ocean (below) (after Tomczak et al, 1994)

The resulting monsoonal climate dominates mainly in the northern Indian Ocean but its effects are still felt well into the Southern Hemisphere (around 20°S) (Tomczak et al, 1994). Off northern Mozambique and Tanzania, the monsoon leads to reversals in wind direction between southeasterly and northwesterly. The main focus of this dissertation concerns the coastal ocean off Tanzania.

The united republic of Tanzania, which includes Zanzibar (Unguja and Pemba Islands), lies south of the equator, between latitudes 4°S to 11°45'S and longitudes 29°21'E to 40°25'E. To its east is the western Indian Ocean. Thus, the Tanzanian coastal ocean and Tanzanian climate in general are greatly affected by the monsoon over the Indian Ocean and its variability. However, the Tanzanian coastline extends for about 800 km and its continental shelf extends between 4 km and 35 km offshore. Several islands exist in the Tanzanian coastal Ocean (e.g., Unguja, Pemba

and Mafia islands and archipelagos such as Lattam, Tutia, Songosongo and Mbudya - Nyandwi et al, 2001).

The Tanzanian continental shelf and neighbouring waters are characterized by the East African Coastal Current (EACC). Strong south-easterly or nearly southerly winds blowing from April to September over the Tanzanian coastal waters help drive the EACC whereas weaker north-easterly and northerly winds in austral summer oppose the EACC. Due to this wind forcing, the intensity of the EACC and ocean properties off Tanzania vary throughout the year.

1.2 Objective and Motivation for Study

Several studies have been conducted in the Tanzanian coastal ocean (Newell, 1957, 1959; Dubi, 1998, 1999, 2000; Julius, 2005). However, these studies have been accompanied by very few models to enhance and improve the skills of understanding and knowledge of the ocean circulation, ocean-atmosphere interaction and coupled biogeochemical-ecosystem-circulation systems. With advances in computing, numerical modelling combines the theories, observations and data in oceanography to avoid difficulties associated with each approach when used separately. As a result, a better understanding of ocean dynamics and properties may occur. This dissertation involves on a numerical modelling study of the coastal ocean off Tanzania (Tanzanian continental shelf waters and the adjacent ocean) in the western Indian Ocean for the domain 5^0N-15^0S and 38-55^0E and seeks to address the following key research questions:

1). How does the annual cycle of the sea surface temperature of the Tanzanian coastal ocean relate to the monsoon winds?

2). How do the transition seasons affect the East African Coastal Current (EACC)?

3). How does the annual cycle of the flow entering the southern parts of the Tanzanian coastal ocean relate to the seasonality in the winds and currents north of Madagascar?

Chapter 2 Literature Review

This chapter provides the literature review of studies of the Tanzanian coastal and continental shelf waters in relation to the adjacent ocean. It includes the remote and local forcing which leads to different responses over the Tanzanian waters and the Indian Ocean as whole. It is useful to study the variability of the coastal ocean off Tanzania within the context of the monsoonal variations, the large scale western and equatorial Indian Ocean circulation; and the El Niño-Southern Oscillation (ENSO) and the Indian Ocean Dipole Zonal Mode (IODZM) climate modes.

2.1 Monsoon Winds over the East African Region

The word 'Monsoon' originated from the Arabic word 'Mausin' meaning seasonal change (Pickard et al, 1990; Krishnamurti, 1996; Gadgil, 2003). It has been used worldwide to describe seasonal reversals in the direction of wind during austral summer and winter seasons over the Indian Ocean and the regions that rim it and it is referred to as the Indian monsoon system. The wind reversal results from the contrast in warming between the Asian landmass, dominated by the Tibetan Plateau which covers about 10^6 km^2 with 5 km mean height and the Indian Ocean during both austral summer and winter seasons (Krishnamurti, 1971a and b). This differential heating as a cause of the Indian monsoon was first suggested by Halley in 1686. It is still regarded as the cause of the Indian monsoon (e.g. Webster, 1987).

In the Southern Hemisphere winter (austral winter) from June to September, the Asian landmass is heated more quickly than the ocean due to its lower specific heat capacity. The high altitude Asian landmass elevates the temperature causing the

surrounding air to rise up due to decrease in its density. This creates low air pressure over the Asian landmass compared to the adjacent ocean surface at lower troposphere which results in a north-south pressure gradient from Madagascar to Arabia of 22hPa (Tomczak et al, 1994). As a consequence of this pressure gradient and the Coriolis effects, the wind blows from southwest to northeast, i.e., from the western Indian Ocean and Arabian Sea towards the Asian landmass (Figure 2.1c). Channeling of the wind by the East African highlands further focuses this South West monsoonal flow. The South West monsoon reaches its peak in July-August and fades away in September-October (Rao and Ram, 2005). It is considered as a continuation across the equator of the Southeast Trades and appears to concentrate in a narrow jet, called the Findlater or Somali Jet (Pickard et al, 1990).

The situation is reversed in the austral summer from December to March. During this time, the Asian landmass cools faster than the adjacent ocean resulting in lower air pressure at lower troposphere over the relatively warmer Indian Ocean surface. At this time, the north-south pressure gradient is from Arabia to Madagascar and barely exceeds 6 hPa. The winds now blow from the northeast from the Asian landmass towards the southwest and the tropical South Indian Ocean again influenced by the Coriolis effects and channeling by the East African highlands (Figure 2.1a). This wind is known as the North East monsoon (Tomczak et al, 1994).

The South West monsoon winds are stronger than the North East monsoon; hence, the annual mean wind pattern looks like a weaker version of the South West monsoon, and the ocean response to the South West monsoon is stronger (Pickard et al, 1990). The monsoonal transitions take place between April/May and

October/November for about a 4 to 6 weeks period during which the winds turn eastward at the equator (figure 2.1b and d).

Although the monsoonal climate dominates the northern Indian Ocean, its effects are felt far into the Southern Hemisphere (Tomczak et al, 1994). Tomczak and Godfrey (1994) and Hermes and Reason (2008) pointed out that the southeast and northwest winds reverse between 12^0S and the equator in austral winter and summer respectively. The Southeast trades persist throughout the year south of about 10 and 12^0S especially in the west. They tend to be the strongest and extend further north during austral winter.

Associated with the monsoon winds over the East African region is the north-south migration of the position of the Inter-tropical convergence zone (ITCZ) (Griffiths, 1959; Nyenzi, 1988; Ogallo, 1989) and cloudbands as mentioned by Gagdil (2003). The ITCZ is the zone in the tropical region where the Northeast trade winds converge with the Southeast trade winds (Grant, 1996). It corresponds essentially to a direct thermal circulation with intense convection, heavy rainfall and low surface pressures over the regions with the highest surface temperatures (Philander, 1999). In austral early summer, the ITCZ appears to be at 2^0S in October and reaches 12^0S by the end of December. It reaches its southernmost location at the end of January / February before moving northward along the East African coast. It is again located at 2^0S by the end of April. Typically, the ITCZ position lags about 4 to 6 weeks behind the time of the sun's maximum elevation (EAMD, 1963b). The sun is approximately overhead in Tanzania by the end of the months of March and September when it moves north and south of equator respectively. As a

consequence, the ITCZ is most influential over Tanzania in late April/May and October/November respectively. It involves convergence of the Southeast and Northeast trade winds. Thus, the northern part of Tanzania receives bimodal rainfall; namely, the long rains (Masika) from March to May (MAM) and the short rains (Vuli) from October to December (OND) (Alusa and Gwange, 1978; Mhita and Nasib, 1987; Kabanda, 1995; Mpeta, 1997; Mwandosya et al, 1998; Dubi, 2000).

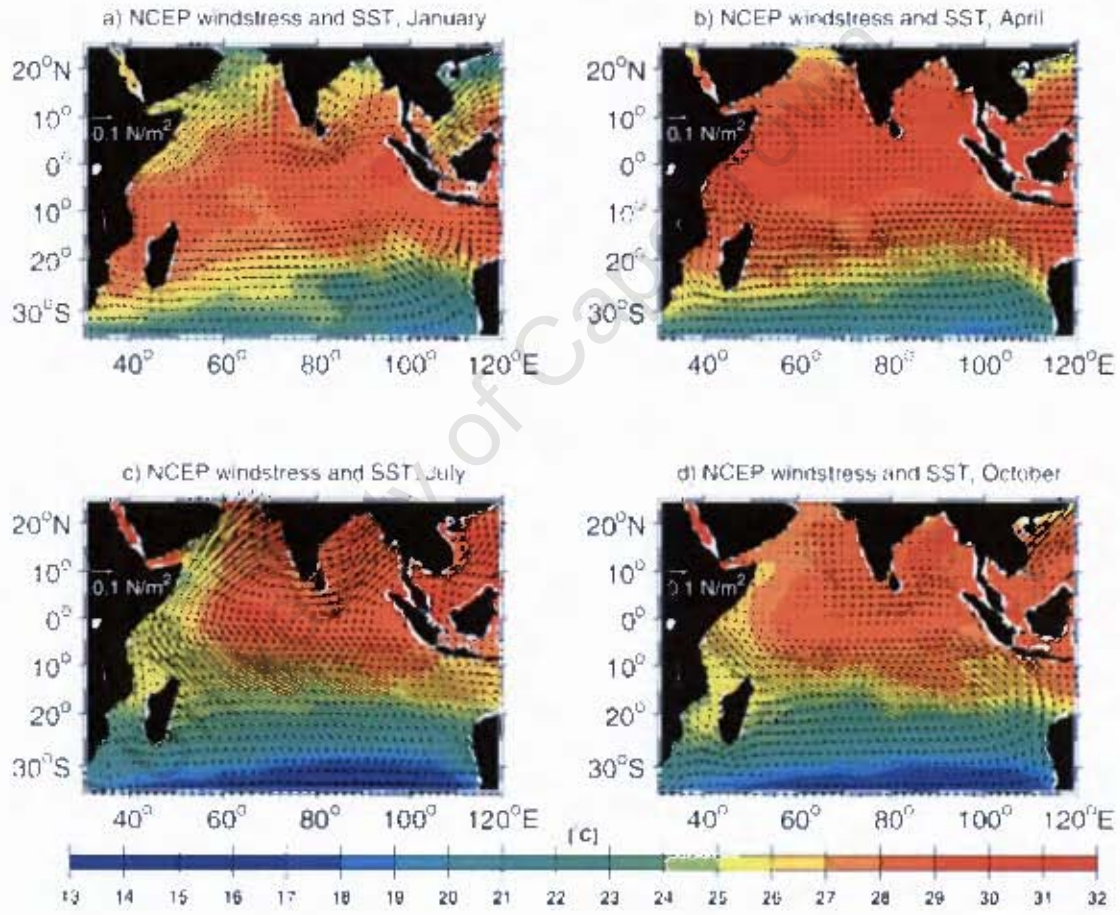

Figure 2.1: Monthly mean wind stress (Nm^{-2}) from NCEP climatology a) January – North East monsoon. b) April- monsoon transition. c) July – South West monsoon. d) October - monsoon transition. Monthly mean surface temperature (°C) from Levitus and Boyer (1994) is shown in color (Schott et al, 2002).

Since the southern part of Tanzania is near the southernmost location of the ITCZ, it experiences only one rainy season from November to April with the peak rains from January to February (EAMD, 1963a and b; Alusa et al, 1973; Mpeta, 1997; Mwandosya et al, 1998).

2.2 Seasonal Variations of Tanzanian Coastal Waters

The winds over the Tanzanian waters considered in this research are those found between 11^0S to the Equator, a part of the western Indian Ocean that is greatly affected by the monsoon winds. From April to October/November, there are the southeasterly or nearly southerly winds that blow over the Tanzanian waters crossing the Indian Ocean towards the Asian landmass. These winds are moist with relatively low temperature (approximately 25^0C) and strong with a constancy of direction (Dubi, 2000). During November to March, the Tanzanian waters experience northeasterly (nearly northerly) light or weak monsoons with high air temperature greater than 30^0C (Newell, 1957; Dubi, 1998; Dubi, 2000; Julius, 2005). The collection and analysis of wind data from 1972 to 1996 by Dubi (1998, 1999) found monsoon winds speeds of 13.5 ms^{-1} for Tanga and 14.5 ms^{-1} for Zanzibar with peak speeds during the North East monsoon. A mean speed of 13.5 ms^{-1} was observed for Dar es Salaam with peak speeds in February, April and July while Mtwara, in southern Tanzania observed an average speed of 18 ms^{-1} with peak winds during the South West monsoon season (July/August).

Further studies have shown that the sea surface temperatures (SSTs) in these waters can range between 26.0-28.0^{0}C in February, 28.0°C in May, between 24.0-

26.0℃ in August, 27.0℃ in November (United Nation Environmental Program (UNEP), 1985; Mahongo, 1999) and between 25-26^{0}C in June and July (Nyandwi et al, 2001). Rao et al. (2005) stated that the SST at 10^{0}S varies from about 29^{0}C (in March-April) to about 26^{0}C (in August) whereas further north, the SST increases from about 28^{0}C in the west to more than 29^{0}C in the eastern part during January-February. Further description on the temperatures of the coastal waters off Tanzania can be found in Newell (1959); Dubi (2000); Francis et al. (2000); Nyandwi et al. (2001) and Julius (2005). Newell (1959) and Julius (2005) pointed out that during the monsoonal transition months of March and April, when the North East monsoon ends, maximum SST of 28-30^{0}C occurs. The minimum SST of 24^{0}C on average occurs in June-September during the South West monsoon.

Studies on the salinity of the Tanzanian waters (Nyandwi et al, 2001) find 34 and 35.2 psu as the typical sea surface salinity values between April and June. Dubi (2000) mentioned that the maximum surface salinity occurs in November and December in the south and north respectively. The minimum surface salinity was found to be in the south during May. The influence of freshwater on coastal salinity is attributed to major and minor rivers along the Tanzanian coast flowing into the ocean. These rivers are like Ruvuma, Mbemkulu, Rufiji, Ruvu and Pangani. Their corresponding outflow of freshwater into the ocean becomes large towards the end of the rainy season and hence they greatly affect the salinity of the coastal waters during that time. The Rufiji river, which is one of the largest rivers in Africa, discharges about 2000-3000m^3/s into the Tanzanian coastal ocean (Dubi, 2000; Shaghude, 2003; and Julius, 2005).

The monthly and seasonal sea level variations over the tropical Indian Ocean including the Tanzanian coastal waters are associated with the prevailing monsoon winds. Kumar (2001) and Singh et al. (2001) pointed out that the prevailing seasonal change of monsoon winds cause the sea level variations at Cochin, the southwest coast of India and at the Maldives coast respectively. Singh (2002) showed that the maximum rise in sea level at Maldives coast occurs during the South West monsoon winds. The Bangladesh coast showed an increase of sea level variations during the South West monsoon when the SSTs over the equatorial region and the North Indian Ocean are significantly high (Singh, 2002). In the western tropical Indian Ocean, the maximum sea level variations are observed during November to April and minimum from May to October which roughly reflects the wet and dry seasons (Ruby and Sete, 2002).

Ngwali (2006) stated that Zanzibar Island in the Tanzanian coastal ocean is characterized by high sea level variations from March to May and October to November. This variation is associated with changes in sea level pressure and insolation which are related to the South West and North East monsoon winds over the East African coast. The highest sea level period occurs in April. He showed that the months of July to August and January to February are characterized by lower sea levels.

The net surface heat flux plays a crucial role in the global climate system because it influences sea surface properties like salinity and temperature. It represents the net heat gain or loss at the ocean surface resulting from the balance between incoming short wave and long wave radiations; the heat loss by outgoing long wave radiations

and through evaporation (latent heat), and to some extent by the surface turbulent fluxes of the sensible heat (Rao et al, 2005). A net surface heat flux of more than 100 Wm^{-2} occurs over the northwestern and western Indian Ocean (north of 10^0S) during March-April and during September-October off Somalia and Arabia. South of 10^0S, a heat loss of $40Wm^{-2}$ occurs during May-August (Rao et al, 2005).

The tropical South Indian Ocean gains heat during the austral summer but it loses heat during the austral winter, whereas most of the equatorial Indian Ocean gains heat throughout the year (Rao et al, 1989). Rao and Sivakumar (2000) showed that during the austral summer; the dry and cold north-easterly winds originating from the Asian landmass lead to strong cooling off the North Indian Ocean especially in the northwest of both Arabian Sea and Bay of Bengal. The influence of light winds and clear sky conditions in the pre-South West monsoon season (the boreal spring transition) results in a high net surface heat gain which warms the ocean region north of 20°S, with increasing amplitude toward the north. A remarkable cooling over the entire tropical Indian Ocean, and particularly over the south-west, results from the net surface heat loss that occurs during the South West monsoon season. However, coastal wind-driven upwelling off the Somali and Arabian coasts leads to cooler SST. During the post-South West monsoon season (austral spring), the net surface heat flux warms the entire Arabian Sea with maxima in the south-western region where the insolation is high and evaporation is low because of the presence of cold upwelled waters at the surface. On the annual average, there is a net heat flux into the Indian Ocean nearly everywhere north of 15^0S which ranges in magnitude between $0.5\text{-}1.0 \times 10^{15}\ Wm^{-2}$ (Godfrey et al, 1995).

2.3 The Indian Ocean Equatorial Circulation

The monsoon winds over the Indian Ocean lead to different equatorial processes compared to the Pacific and Atlantic Oceans (Stewart, 2007). On either side of the equator, the Pacific and Atlantic Oceans are mostly dominated by easterly winds (Tomczak et al, 1994) which lead to westward currents throughout the year. The situation is different in the Indian Ocean due to the presence of the monsoon. As a result, the Indian Ocean equatorial regime experiences four reversals of direction of the currents throughout the year influenced by the South West, North East and transition season monsoons. Schott et al. (2001) discussed how the equatorial currents flow westward in winter, weakly westward in the central and western ocean in summer, and strongly eastward during the spring and autumn. The eastward equatorial current occurs during the monsoon transition months (May and November) when the winds turn eastward at the equator, producing Ekman convergence. Basically, the eastward winds along the equator force the eastward flowing currents in April-May and October-November of each year (McPhaden et al, 2008). These eastward flowing currents in spring and autumn are known as the Equatorial or Wyrtki Jets named after Wyrtki, the first person who identified them (Wyrtki, 1973).

The Equatorial (or Wyrtki) Jets have been shown by Schott et al. (2001) to affect the sea surface temperature, mixed layer and sea level across the equatorial Indian Ocean. Furthermore, Schott et al. (2001) observed that two months after the onset of the Equatorial Jets, upper surface waters are transported from west to east decreasing the mixed layer, sea surface level and surface temperature in the west

while increasing them in the east. Thus, these jets play an important role in the seasonal heat balance of the Indian Ocean basin (McPhaden et al, 2008).

Furthermore, when the currents arrive at the end of the basin in the east, some of the transported waters are reflected towards the west to propagate as Rossby waves as observed in the 2-layer model by O'Brien and Hurlburt (1974). Some waters reflect poleward and, hence, impact the Bay of Bengal (Schott et al, 2001). The Wyrtki Jets are estimated to have a strength of about 1 ms^{-1} in autumn and spring. Model studies using realistic wind data by Anderson et al. (1993); Jensen (1993) and Han et al. (1999) using two different wind stress forcing showed that the Wyrtki Jets are weaker in autumn than in spring.

The increase of sea surface level in the east, attributed to the equatorial jets, generates a subsurface pressure gradient force due to water column differences. The subsurface pressure in the east is higher than that in the west causing a westward pressure gradient force. This pressure gradient force results in the undercurrent flowing in the opposite direction of the surface current. Hence, the Surface Equatorial Current causes the Equatorial Undercurrent (EUC) to flow westwards.

It has been reported that the westward flowing Equatorial Undercurrent can be only observed consistently during austral autumn (Schott et al, 2001) and in different depth and locations along the equatorial Indian Ocean (e.g. Taft, 1967; Swallow, 1967; Knox, 1976; Leetmaa and Stommel, 1980; Reppin et al, 1999). Nevertheless, Leetmaa and Stommel (1980) confirmed the existence of the EUC meandering more

than 100 km south of the equator. Using a numerical model, Jensen (1991) showed the westward undercurrent begins in May and persists throughout the South West monsoon.

In addition, the Indian Ocean experiences a seasonal North Equatorial Current (NEC) which is prominent in January and March when the North East monsoon is fully established; and a permanent South Equatorial Current (SEC) due to the Southeast Trades. The North Equatorial Current is formed when the North East Monsoon current (NMC) persists through March (Hacker et al, 1998; Schott et al, 2001) (Figure 2.2). It runs as a narrow current of about 0.3 ms^{-1} from the Malacca Strait to Southern Sri Lanka where it bends southward and accelerates to reach 0.5-0.8 ms^{-1} between 2^0S and 5^0N in the region between 60^0E and 75^0E. The South Equatorial Current (SEC) is found between 10^0S and 20^0S (Cutler and Swallow, 1984; Shenoi et al, 1999) with velocities rarely exceeding 0.3 ms^{-1} (Tomczak et al, 1994). The SEC carries fresh water from the Indonesian Passages westward. Its path is more irregular due to the effects of the underlying topography and Rossby waves as shown by the high-resolution Parallel Ocean Program Model (POP) described by Maltrud et al. (1998) and Gordon and McClean (1999). The SEC bifurcates at the coast of Madagascar at about 17^0S, generating the Northeast Madagascar Current (NEMC) and the Southeast Madagascar Current (SEMC) to the north and south respectively (figure 2.2). The NEMC moves northwestward past Cape Amber with an estimated annual mean of 29.6±8 Sv (Swallow et al, 1988) with near-surface speed of 70cms^{-1} which decays monotonically down to a depth of 1000 m (Schott et al, 2001). On reaching the southern Tanzanian coast, it splits

again into a southward flow through the Mozambique Channel and a northward flow as the East African Coastal Current (EACC) (Pickard et al, 1990; Tomczak et al, 1994).

Between the NEC and the SEC there is the eastward flowing South Equatorial Countercurrent (SECC) (Figure 2.2b) which is formed by the confluence of the northward flowing EACC and the southward flowing Somali Current at about 2-3^{0}S (Düing & Schott, 1978) during the North East monsoon. It has also been suggested that the SECC results from the merging of these westward flowing currents causing the geostrophic balance with meridional density contrast in the Seychelles-Chagos thermocline ridge region (Hermes and Reason, 2008; Yokoi et al, 2008). The EACC and Somali Current will be described in the next section. The velocities of the SECC are between 0.5-0.8 ms^{-1} in the west but weaker in the east. It does not go beyond 70^{0}E in January, being opposed in the east by a weak westward flow. It is best developed in February when it forms a continuous band across the Indian Ocean, causing high sea level in the east at this time (Morrow & Birol, 1998).

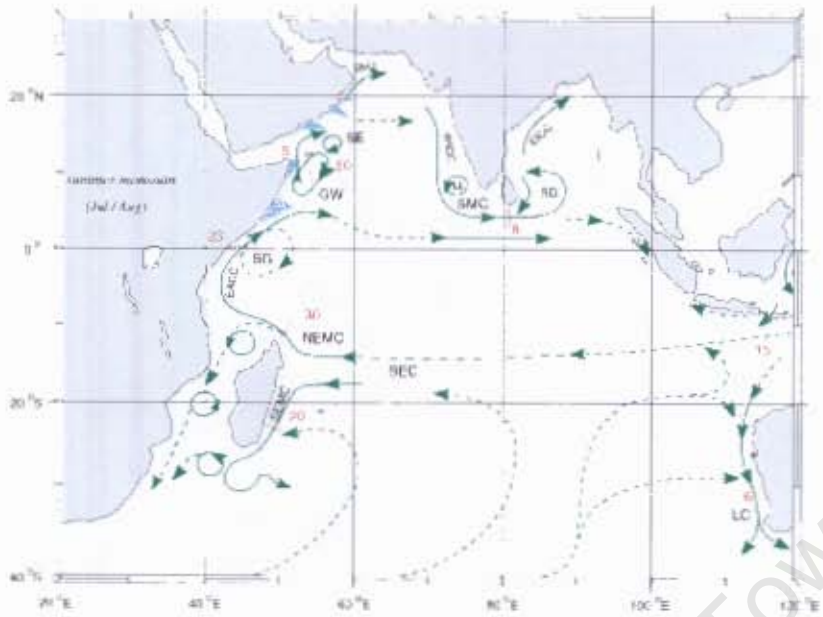

(a)

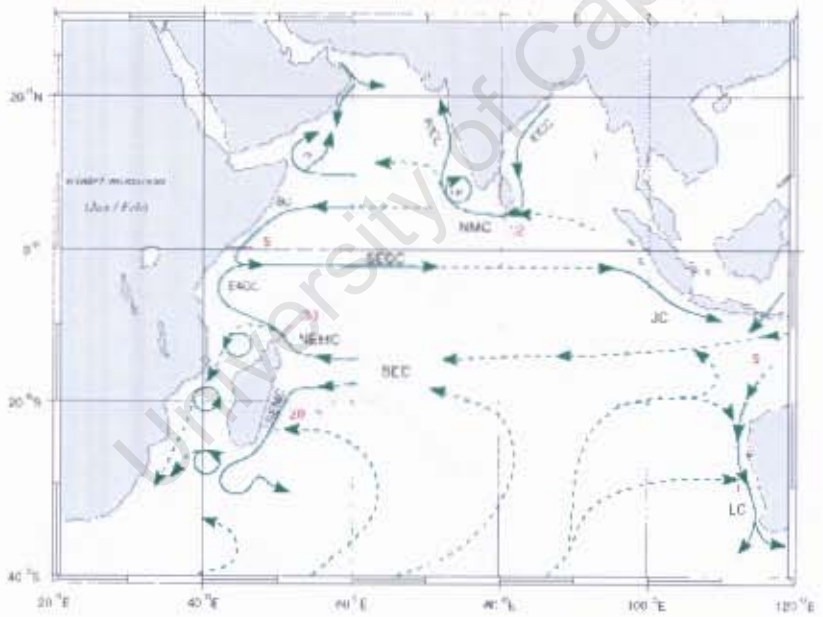

(b)

Figure 2.2: Indian Ocean circulation in the response to (a) South West monsoon and (b) North East monsoon (after Schott & McCreary, 2001).

2.4 The East African Coastal Current (EACC)

Tomczak and Godfrey (1994) described the East African Coastal Current (EACC) or the Zanzibar Current (ZC) as the permanent northward flowing current from about 10^0S fed by the Northeast Madagascar Current (NEMC). Swallow et al. (1991) considered approximately 3^0S as a northern limit of the EACC instead of equator which was suggested by Newell (1957). The Northeast Madagascar Current, which originates from the SEC bifurcation, moves northwestward to where it meets the mainland of the southern Tanzania. It then splits north and south generating the permanent EACC and Mozambique Current (MC) respectively with seasonal speed variations (Swallow et al, 1991; Julius, 2005). Although previously shown as a coherent current (Figure 2.3), the flow through the Mozambique Channel exists more as a train of eddies rather than as a distinct current (Biastoch et al, 1999; Lutjehams et al, 2000; de Ruijter et al, 2006). The intensity of the EACC is influenced by the monsoon winds and the southward flowing undercurrent.

During the North East monsoon season when winds blow from the Indian subcontinent towards East Africa, the EACC is opposed by light winds and the southward flowing Somali Current, and hence it is weakened. Thus, during the November to March period, the EACC has an average velocity of less than $0.2ms^{-1}$ (Newell, 1957; Dubi, 2000; Julius, 2005). The EACC and Somali Current meet each other near 3^0S (Swallow et al, 1991) but this confluence can range from 1^0 N at the beginning of austral summer to 4^0S during February, when the EACC is at its weakest (Tomczak et al, 1994). Thereafter, the confluence zone starts to move

northward and reaches the equator by early April. Throughout this period, the EACC feeds into the South Equatorial Countercurrent (SECC).

During the South West monsoon, the Southeast trade winds help drive the EACC northward flow and lead to a considerable increase in its strength. In this season (April to October), the EACC attains its strongest speeds and can reach a velocity of up to $2ms^{-1}$ with a tendency of being deflected out to sea (Newell, 1957; Dubi, 2000; Julius, 2005). Speeds of $2.0ms^{-1}$ were also reported during INDEX observations from April/May 1979 with the transport of 15Sv as stated by Schott et al. (2001).

However, Swallow et al. (1991) argued that there is a rapid increase of the monthly mean northward components of the surface current in April, up to July after which the flow decreases slowly through the rest of the year (Figure 2.4). Furthermore, Swallow et al. (1991) noted that there is also an increase in the mean northward speed of the EACC in austral winter from 10^0S towards the equator regardless of the complication provided by the Islands of Mafia, Unguja and Pemba in its path. The width of the EACC suggested by Bell (1972) on fishery research cruises from Zanzibar at 6^0S is over 160km with maximum speeds found between 16 and 80 km offshore. During the South West monsoon, the EACC feeds the northward flowing Somali Current and some consider it as a part of the Somali Current during these months.

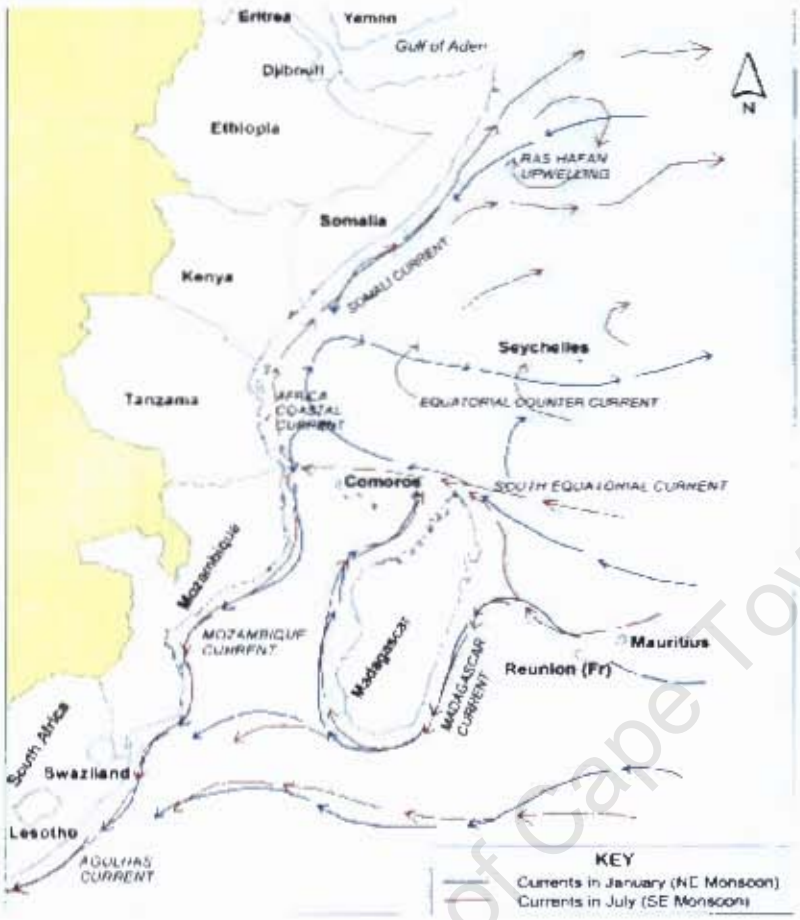

Figure 2.3: A traditional schematic of the ocean currents in the western Indian Ocean (Julius, 2005, Ruitenbeen et al, 2005)

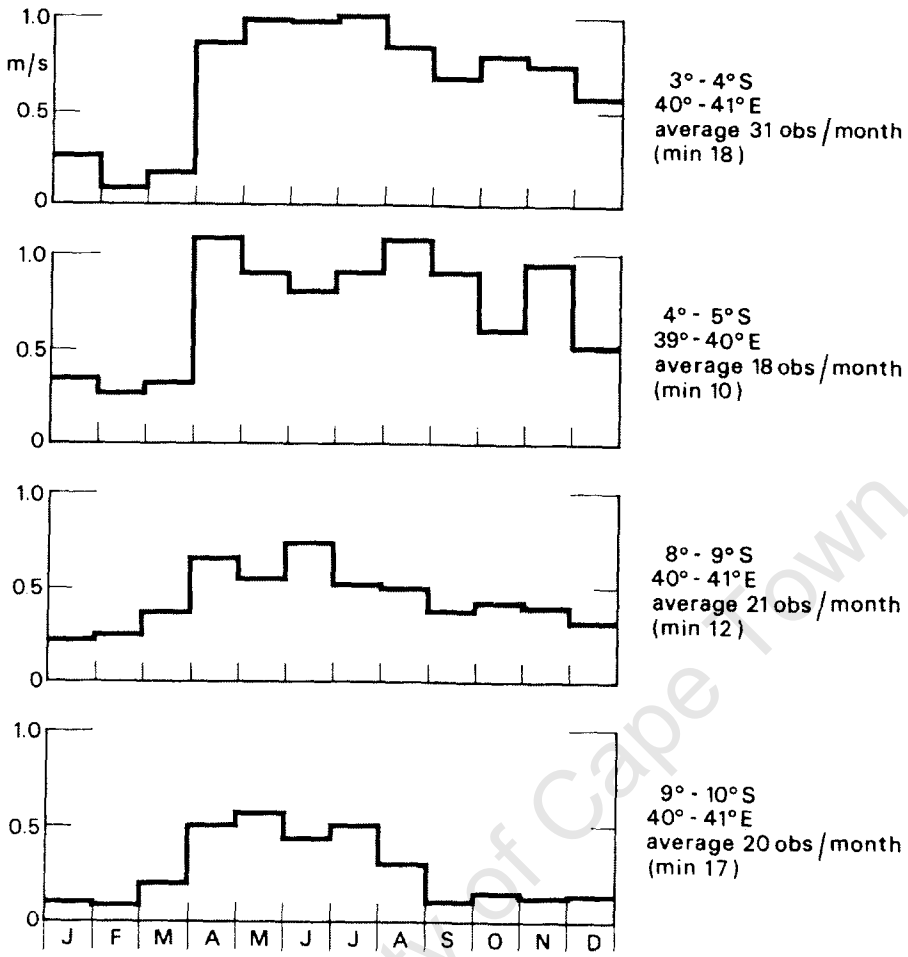

Figure 2.4: Seasonal cycle of monthly mean northward component of the historical ship drift currents at selected latitudes in EACC (Swallow et al, 1991).

2.5 The Somali Current

The Somali Current is formed as an extension of the EACC that flows northward across the equator to about 3-4^{0}N before the South West monsoon. It is fully developed during the South West monsoon when it is considered to be one of the fastest open-ocean currents in the world. It is associated with different large,

recurrent eddy structures such as the Southern Gyre, Great Whirl and Socotra Gyre (or eddy).

As shown in Figure 2.5, after the Somali current crosses the equator, one part turns offshore at 4^0N with a width of order 50-100 km, generating upwelling further north (Pickard et al, 1990; Schott et al, 2001). The northward flow coming from the south bifurcates at 4^0N off the coast turning to the east and south towards the equator, thereby forming the Southern Gyre which varies in strength from year to year (Schott et al, 1990). This bifurcation takes place between March and May and the offshore turning leads to a cold wedge along its inshore part. During June and July, following the sudden onset of the South West monsoon, westward propagating Rossby waves (Quadfasel et al, 1982) are generated in the equatorial Indian Ocean. These waves cause energy accumulation at the west coast. Further north at 4-10^0N, the Great Whirl develops due to very strong anti-cyclonic wind stress curl generated offshore from the Somali coast which results in another cold wedge at latitudes 10-12^0N. Moreover, the formation of the Great Whirl precedes the formation of the Southern Gyre (Pickard et al, 1990) with very little exchange in water mass between them. Another smaller recurrent eddy known as the Socotra Gyre (or Eddy) is also formed at about 12^0N (Pickard et al, 1990; Schott et al, 2001).

During the late South West monsoon, August to September, there is a complete closed Great Whirl with very small exchanges with the offshore flow. The last phase is when the South West monsoon dies down from October to November leading to the Great Whirl maintaining its closed circle and the cross-equatorial Somali Current

turning offshore again at 3°N. These phases are depicted in Figure 2.5 in March-May, June-July, August September, October-November and December-January.

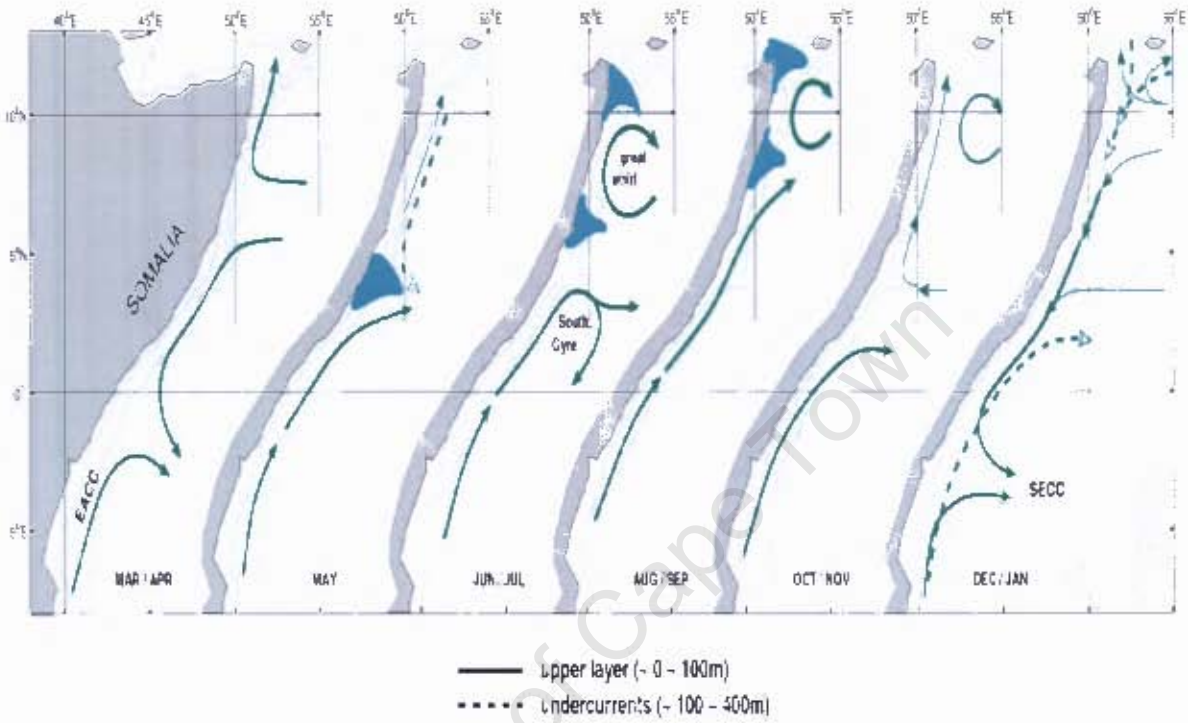

Figure 2.5: Schematic diagram of the Somali Current phases throughout the year (after Schott et a , 1990; Schott et al, 2001).

During the North East monsoon, the surface Somali Current reverses to flow southward and is now forced by the North East monsoon winds blowing off the Indian Subcontinent As a consequence, the confluence of the Somali Current with the East African Coastal Current (EACC) occurs near 3°S (Swallow et al, 1991). Subsequently, there is an eastward offshore flow at 2°S to 4°S (Düing & Schott, 1978; Schott et al, 2001) which results in the South Equatorial Countercurrent (Figure 2.2b and 2.3).

Bell (1972) and McClanahan (1988) pointed out that the Tanzanian coastal waters and southern Kenyan waters experience downwelling throughout the year and the Somali coast experiences upwelling during the South West monsoon (Warren, 1966; Warren et al, 1966; Düing & Schott, 1978; Smith & Codispoti, 1980; Leetmaa et al, 1982). Thus, the southern area (Tanzanian and southern Kenyan coasts) is dominated by coral reefs and benthic productivity associated with low-nutrients water while the northern part (Somali and northern Kenyan coasts) is dominated by planktonic rich-nutrients waters and productivity.

2.6 El Niño-Southern Oscillation (ENSO) and Indian Ocean Dipole-Zonal Mode (IODZM)

The most prominent inter-annual variability affecting the Indian Ocean is the El Niño-Southern Oscillation (ENSO) that originates in the tropical Pacific Ocean (Reason et al, 2000; Yamagata et al, 2004; McPhaden et al, 2008; Schott et al, 2008). Within the Indian Ocean, another prominent mode is the Indian Ocean Dipole Zonal Mode (IODZM) (Saji et al, 1999; Webster et al, 1999). The ENSO leads to an anomalous increase of sea surface temperatures and sea surface height in the eastern tropical Pacific Ocean and opposite in the west. It originates in the tropical Indo-Pacific Ocean with large global climate impacts (Diaz et al, 2000). It affects the climate variability (Parker, 1992; Reason et al, 2000) by changing the oceanic and atmospheric parameters such as sea surface height and temperature in the tropical oceans (Bjerknes, 1966; Hickey, 1975; Ropelewski et al, 1987; Philander, 1990; Phinn et al, 1992).

Stewart (2007) described the forcing and dynamic processes taking place in the evolution of ENSO as follows: The trades the equatorial Pacific Ocean (and particularly in the west) weaken and sometimes reverse direction producing westerly wind bursts. This weakening quickly deepens the thermocline in the west launching an eastward propagating Kelvin wave along the equator. This wave deepens the thermocline and carries warm water eastward for about three to four months to reach the western coast of South America. Thus, relatively warm water upwelled in the upwelling region in the western equatorial Pacific Ocean deepens the thermocline there. This process causes surface temperatures offshore of Ecuador and Peru to warm by 2-4^{0}C. The warm water reduces the temperature contrast between east and west, leading to a further reduction of the trades and the rapid development of El Niño. The change of the sea surface temperature causes the convergence zone along the equator to shift eastward from Melanesia and Fiji to the central Pacific leading to a widespread warming zone. The widespread warming zone leads to an increase of exchange of angular momentum with the neighboring subtropical belt, whereby the subtropical westerly jet strengthens (Bjerknes, 1972) and atmospheric Rossby waves are generated, thereby resulting in global impacts.

When the Kelvin wave reaches the coast of Ecuador, part is reflected as a westward propagating Rossby wave, and part propagates north and south as coastal trapped Kelvin waves carrying warm water to higher latitudes. As the Kelvin wave moves along the coast, it generates other Rossby waves which move west across the Pacific with a velocity that depends on the latitude. The velocity is very slow at mid to high latitudes and fastest on the equator. There the reflected wave (Rossby wave)

moves back as a shallowing of the thermocline, reaching the central equatorial Pacific a year later. In a similar way, the westward propagating Rossby wave launched at the start of the El Niño in the west, reflects off Asia and returns to the central equatorial Pacific as a Kelvin wave, again about a year later (Figure 2.6).

This time, however the waves decrease the sea-level and sea surface temperature returning the area to neutral or La Niña conditions. El Niño ends when the Rossby waves reflected from Asia and Ecuador meet in the central Pacific about a year after the onset of El Niño (Picaut et al, 1997). The waves push the warm pool at the surface toward the west. At the same time, the Rossby wave reflected from the western boundary causes the thermocline in the central Pacific to become shallower when the waves reach the central Pacific.

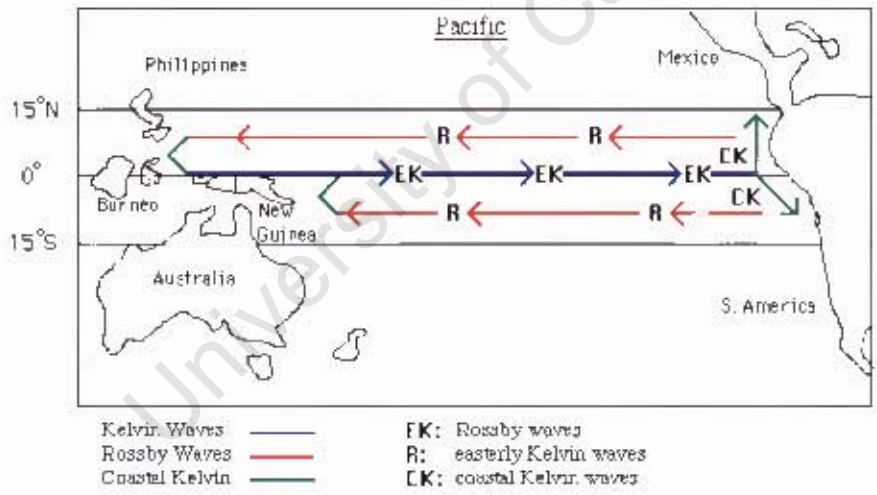

Figure 2.6: Propagation of Kelvin and Rossby waves in equatorial Pacific Ocean. (http://library.thinkquest.org/3356/main/course/moreintro.html)

Then, any strengthening of the trades causes upwelling of cold water in the east, which increases the east-west temperature gradient, strengthening the trades, and

hence increasing the upwelling (Takayabu et al, 1999). The system is then thrown into the La Niña state with strong trades, and a very cold tongue along the equator in the east. La Niña tends to last longer than El Niño, and the cycle from La Niña to El Niño and back takes about three years. The cycle is not exact. El Niño comes back at intervals from 2-7 years, with an average near four years.

The eastward shifting of the convergence zone along the equator of the Pacific Ocean during the ENSO attributes to anomalous subsidence, suppressed convection, high atmospheric surface pressure and anomalous easterlies over the Indian Ocean. As a result, changes in the precipitation occur over the Indian Ocean and countries surrounding its basin like Tanzania. In Tanzania, El Niño years tend to experience an increase of rainfall over its northern coast (Kijazi and Reason, 2005) with the opposite tendency to occur in La Niña years. Furthermore, different authors have described the variations in different climatic parameters over the Indian Ocean region associated with ENSO. These include strong drought or floods (Allan et al, 2003), sea surface anomalies in winter and spring (Yu et al, 2002). Also, the warming over the tropical Indian Ocean basin in the boreal spring following the peak El Nino (Xie et al, 2002; Yu et al, 2005; Schott et al, 2008) which persist into the following boreal summer, increasing rainfall over the basin (Yang et al, 2007). Furthermore, ENSO increases sea level height over the East African coastal waters (Chamber et al, 1999; Ngwali, 2006). In 1997/1998, a particularly strong El Niño occurred at the same time as a positive phase Indian Ocean Dipole Zonal Mode event leading to very strong warming in the Indian Ocean and flooding in East Africa.

The Indian Ocean Dipole-Zonal Mode (IODZM) is also an interannual climatic variability of the tropical Indian Ocean region depending on conditions set by monsoonal circulation (Loschnigg et al, 2003). In its positive phase, positive sea surface temperature anomalies (SSTAs) occur over the western side and negative sea surface temperature anomalies (SSTAs) over the eastern side of the Indian Ocean. Roughly, the reverse pattern occurs during its negative phase (Figure 2.7).

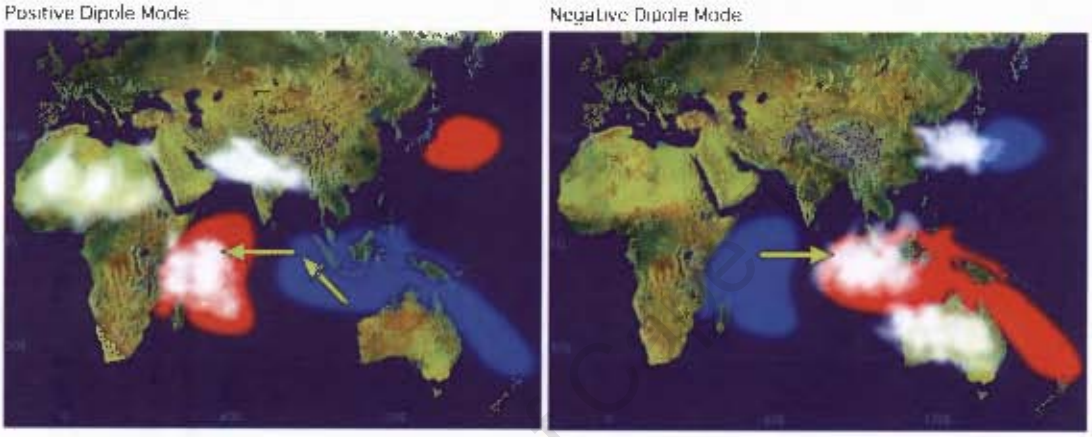

Figure 2.7: The positive (left) and negative (right) phase of Indian Ocean Dipole-Zonal Mode. (http://www.jamstec.go.jp/frsgc/research/d1/iod/)

When the IODZM is positive, East Africa including Tanzania tends to experience above average rainfall during October to December while Indonesia and Australia experience relatively dry conditions (Ashok et al, 2004). The IODZM years are shown in figure 2.8 and the most recent positive IODZM years which are associated with the above average rainfall in the western Indian Ocean / East Africa are 1994,1997 and 2006 (McPhaden et al, 2008). During negative IODZM phase, the SST pattern leads to relative stability in the atmosphere over East Africa and drought whereas East Asia tends to experience heavy rainfall (Behera and Yamagata, 2001).

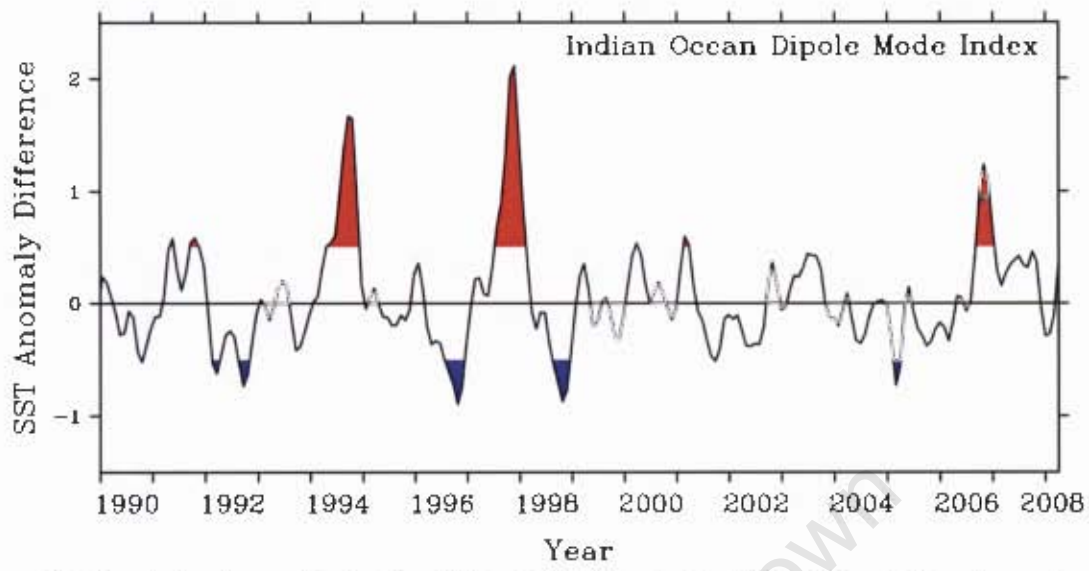

Figure 2.8: The Indian Ocean Dipole Zonal Mode (IODZM) index for 1990-2008, with the strongest positive events (index > 0.5°C) and negative events (index < -0.5°C) highlighted in red and blue respectively (After McPhaden et al, 2008)

However, Alory et al. (2007), McPhaden et al. (2008) and Schott et al. (2008) suggested that positive IODZM phase tends to co-occur with El Niño and negative IODZM phase tends to co occur with La Nina. When both modes coincide, particularly with high positive sea surface temperature anomalies and sea level anomalies in the tropical western Indian Ocean, very heavy rainfall tends to occur over the East African region during the austral spring and summer as in 1997/98 (Saji and Yamagata, 2003).

It has been shown that Zanzibar, off the Tanzanian coast, experiences inter-annual sea level variations particularly during ENSO and IODZM years (Ngwali, 2006). For example, strong positive sea level height anomalies coincided with the 1997/1998 El Niño / positive IODZM event and negative anomalies coincided with the 2000/2001 La Nina year.

To date, there has been very little modelling of the coastal ocean off Tanzania. This dissertation applies the Regional Ocean Model Systems (ROMS) to the Tanzanian coastal ocean and adjacent waters. The model studies are geared towards a better understanding of the annual cycle of the sea surface temperature in relation to monsoon winds and the strength of the EACC during the monsoonal transitional seasons i.e. April/May and October/November months. Also, the annual cycle of the flow entering the southern part of the Tanzanian waters which feeds the East African Coastal Current is studied in relation to the seasonality north of Madagascar.

Chapter 3 Data and Methodology

This chapter provides discussion of the data and methods used in the numerical modeling studies of the Tanzanian continental shelf waters and the adjacent ocean. The monthly climatology derived from January 1945 to December 1989 Comprehensive Oceanic and Atmospheric Data Set (COADS) (Da Silva et al. 1994) has been used to force the ROMS model for ten years and the results are visualized using MATLAB software. The SST model output was compared with the sea surface temperature satellite data derived from the Tropical Rainfall Measuring Mission (**TRMM**) Microwave Imager (**TMI**) measurements for the same region. Further details on the data and methodology are provided below.

3.1 Ocean Model

3.1.1 Regional Oceanic Modeling System (ROMS)

The **R**egional **O**ceanic **M**odeling **S**ystem **(ROMS)** is a numerical code developed at Rutgers University and at the University of California, Los Angeles in USA as an improvement of S-Coordinates Rutgers University Model (SCRUM). It is a free-surface, terrain-following ocean model which solves the three-dimensional hydrostatic primitive equations including the non-linear terms (Shchepetkin and McWilliams, 2003, 2005) and tangent linear and adjoint terms (Moore et al, 2004). It solves the equations using a split-explicit time-stepping scheme and a free-surface with sigma vertical coordinates over variable topography. Stretched, terrain-following coordinates are used in the vertical and orthogonal, curvilinear coordinates are applied in the horizontal on a staggered Arakawa C-grid. In incorporating the

hydrostatic and Boussinesq approximations, ROMS allows the barotropic (fast) mode to be resolved using short time steps and the baroclinic (slow) mode to be resolved using large time steps (Shchepetkin and McWilliams, 2005) for computational economy. This time-splitting allows enhancement of the spatial resolution in regions of interest at reasonable computational cost (Song and Haidvogel, 1994; Penven et al, 2001). Active open boundaries connect the regional model to the open ocean.

The vertical mixing parameterization in ROMS can be either via local or nonlocal closure schemes. The local closure schemes are based on the level 2.5 turbulent kinetic energy equations by Mellor and Yamada (1982) and the Generic Length Scale (GLS) parameterization by Umlauf and Burchard (2003). The nonlocal closure scheme is based on the K-profile, boundary layer formulation by Large et al. (1994). The K-profile scheme has been expanded to include both surface and bottom oceanic boundary layers. The GLS is a two-equation turbulence model that allows a wide range of vertical mixing closures, including the popular k-kl (Mellor-Yamada level 2.5), k-e, and k-w schemes. Several stability functions (Galperin et al, 1988; Kantha and Clayson, 1994; Canuto et al, 2001) have been also added to provide further flexibility. A recent study (Warner et al, 2005) evaluated the performance of these turbulence closures in ROMS in terms of idealized sediment transport applications. In addition, there is a wave/current bed boundary layer scheme that provides the bottom stress (Styles and Glenn, 2000) and sediment transport which become important in coastal applications.

ROMS is free access software and it can be used to assess the different physical processes in the ocean individually and in several coupled models like biogeochemical, bio-optical, sediment and sea ice applications with quite accurate results. Thus, ROMS is extensively used by a large number of people in the community in different scientific applications of worldwide ocean modelling (e.g. Haidvogel et al, 2000; Penven et al, 2001; Di Lorenzo, 2003; Marchesiello et al, 2003; Peliz et al, 2003; Penven et al, 2005; Warner et al, 2005; Wilkin et al, 2005; Colberg and Reason, 2006; Penven et al, 2006). An earlier attempt has been made to install and use ROMS at the Institute of Marine Sciences (IMS), University of Dar es Salaam in 2007 to perform an idealised model of the Zanzibar Channel (Mayorga-Adame, 2007).

ROMS has extensive pre and post-processing software for data preparation, analysis, plotting, and visualization. The entire input and output data structure of the model are in the Network Common Data Format (NetCDF) which allows showing and porting of data by different users or in different machines and software. This facilitates the interchange of data and particularly the ROMS output between computers, the user community, and other independent software. Therefore, the output of ROMS can be analyzed, plotted or visualized through different computer/machine from that used for running model or different software like MATLAB or Ocean Data View (ODV).

3.1.2 Set-up and Configuration of ROMS

A 10 year simulation using climatological forcing over the western Indian Ocean is analyzed in this dissertation with focus placed on the coastal ocean off Tanzania (Tanzanian continental shelf and the adjacent ocean). A ten year long integration appears to be a reasonable period for the model simulation to reach spin-up in response to the forcing and/or to achieve statistical quasi-equilibrium (Penven et al., 2007). The domain of the study extends from 5^0N to 15^0S and 38^0E to 55^0E over the western Indian Ocean (Figure 3.1). The resolution of 1/6 degrees regular horizontal and the vertical resolution consist of 32 sigma coordinate vertical levels used in the model set up. The standard ROMS bathymetry was used for the region.

The atmospheric forcing of the model is obtained from the monthly climatology of the Comprehensive Ocean-Atmosphere Data Set (COADS) (Da Silva et al., 1994 in Penven, 2000). It includes monthly climatologies of heat flux, freshwater flux, surface atmospheric density and temperature, wind speed at 10m, sea level, specific humidity, sea surface salinity and short wave radiation (heat and salt fluxes). The sea surface temperature is computed by the model at each iteration, which in turn is used in the calculation of the restoring force of the heat flux (Penven et al, 2001).

3.2 Datasets and Methods

The ROMS model was forced with the surface marine monthly climatology wind stresses and heat fluxes derived from individual observations in the Comprehensive Ocean-Atmosphere Data Set (COADS) from January, 1945 to December, 1989. They are analyzed on 1^0-by-1^0 global grid and used as the main forcing for the study

domain as shown in Figure 3.1. Satellite derived (TMI-weekly) SST data were used to compute monthly sea surface temperatures over the Tanzanian waters to qualitatively compare against the model.

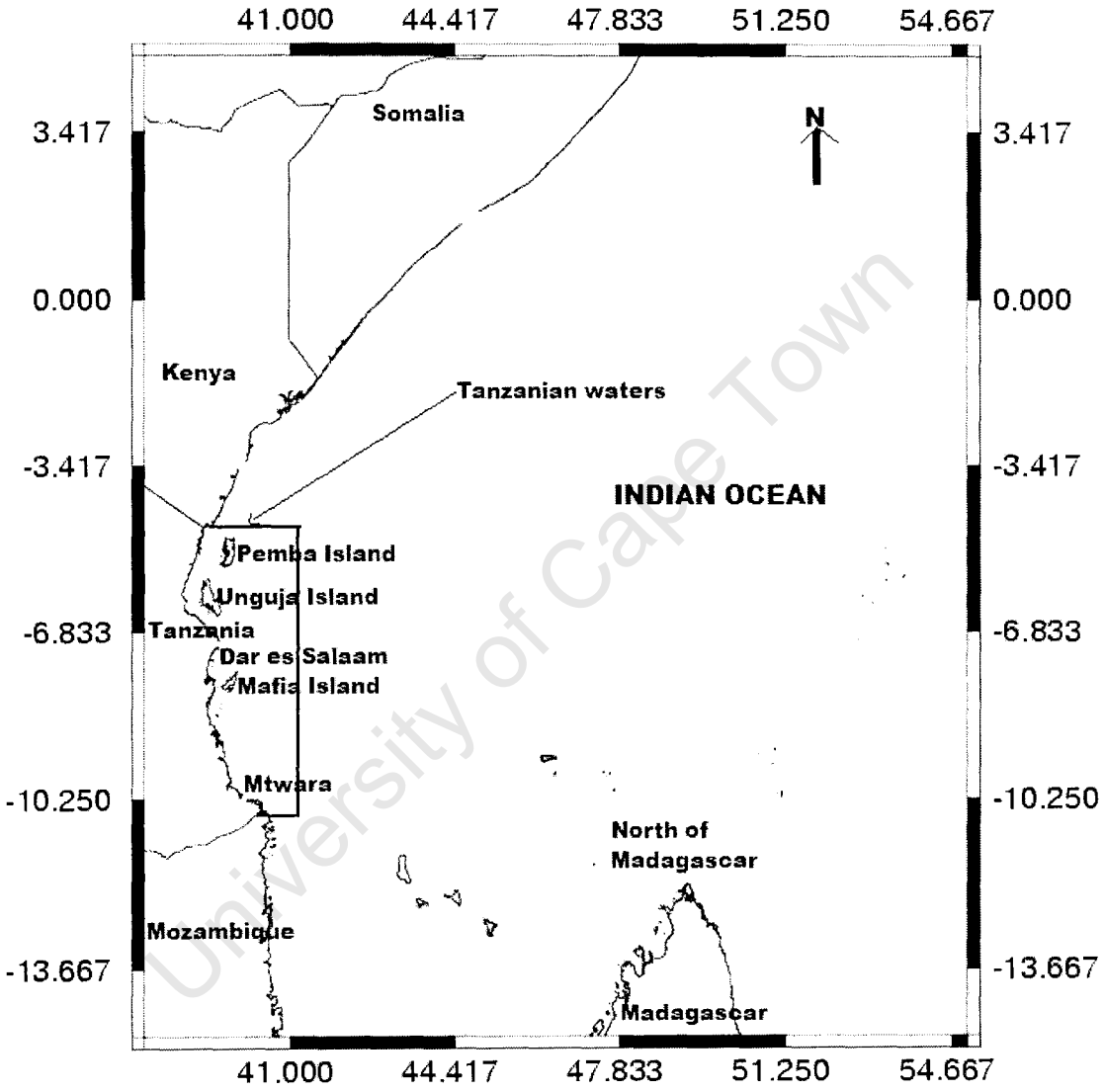

Figure 3.1: The map of the domain region of the study of the Tanzanian waters. (http://rimmer.ngdc.noaa.gov).

Matrix Laboratory (MATLAB), a highly technical computing programming language is used to analyse and display the model results, which are in netCDF format and TMI-SSTs data. The model output statistics (MOS) and plots are done using programming scripts written for that purpose. The embedded roms_gui MATLAB package, which contains different MATLAB scripts for diagnosing and displaying, was used for statistical and visualisation purposes of the model output

3.3 Analysed Variables and Ocean Processes

3.3.1 Wind Stress

Wind stress (kgm^{-1} or Nm^{-2}) is the horizontal force of the wind acting on the sea surface. It is an important driving force for coastal and upper ocean currents whereby it transfers momentum from the atmosphere to the ocean. It has been estimated by using the bulk formulation:

Equation 3.1.....$\tau = (\tau_X, \tau_Y) = \rho C_D W_{10}(u, v)$;

Where W_{10} is the surface wind speed at 10 meters, u is the zonal component (eastward) and v is the meridional component (northward) of wind velocity. The surface wind is assumed to be parallel to the stress vector. ρ is the density of surface air and is always assumed to be constant at 1.3 kgm^{-3} and C_D is the drag coefficient.

The magnitude of the wind stress is:

Equation 3.2.....$|\tau| = \rho C_D W^2_{10}$

The drag coefficient estimation recommended by Smith (1988) and chosen by the WOCE community and largely used in calculation of the magnitude of the wind stress is used. The 10m neutral coefficient formulation over the ocean is

Equation 3.3.....$CD=a+bxW_{10}$

The values of a and b are determined for each wind speed range. The typical values for drag coefficient are between: $C_D=1.5 \times 10^{-3}$ and $C_D=0.5 \times 10^{-3}$.

3.3.2 Geostrophic currents

Geostrophic current is the flow caused by the balance between the Coriolis force and the pressure gradient force. In the models, the geostrophic approximation is used to obtain the horizontal currents. It is represented by the following equations:

Equation 3.4.....$$-\frac{1}{\rho}\frac{\partial p}{\partial x}=-fv$$

Equation 3.5.....$$-\frac{1}{\rho}\frac{\partial p}{\partial y}=+fu$$

Where $\frac{\partial p}{\partial x}$ and $\frac{\partial p}{\partial y}$ are pressure gradients in x and y-directions respectively, u and v are velocity components in x and y-directions respectively, ρ is density of water and f is Coriolis parameter.

Equation 3.6..... $f=2\Omega\sin(\lambda)$

In equation 3.6, $\Omega=7.292 \times 10^{-5}\ s^{-1}$ is the rotation rate of the Earth and λ is latitude (positive in the Northern hemisphere and negative in the Southern Hemisphere).

The Coriolis force (parameter) disappears as one gets close to the equator and the geostrophic formulation does not hold. Thus, an approximation of the equatorial currents is obtained by extrapolation of the currents outside an equatorial band (2^0S – 2^0N).

Chapter 4 Results and Discussion

This chapter discusses the results from the ten years model simulation of the Regional Ocean Model System (ROMS) that was forced with the monthly climatology winds and heat fluxes derived from COADS. These results include the model monthly mean output heat flux, sea surface temperatures for the East African coastal ocean and the East African Coastal Current (EACC). The model output sea surface temperatures are compared to those derived from the Tropical Rainfall Measuring Mission (**TRMM**) Microwave Imager (**TMI**) satellite for the same region.

4.1 Annual cycle of sea surface temperature and net heat flux

It is convenient to begin the discussion of the annual cycle during the month of May because it is the transition period between the onset of the South West monsoon and the end of the North East monsoon. By this month, the relatively cool SST zone (between 27^0C and 28^0C) is apparent to the southeast of the study domain (east and north of Madagascar) in both model results and TMI-SST (Figure 4.1b, c) and it seems to reflect the SEC and NEMC. The tongue of SST of about 28^0C appears to extend from the NEMC moving northward along the East African coast and it reflects the EACC. The SSTs off the Tanzanian coast appear to be about 28^0C during this month as observed by UNEP (1985). The SST increases from 29^0C to 31^0C from 8^0S towards the northeast of the study domain, bounded by the SEC, NEM and EACC in the south and west; and by the Horn of Africa. The net sea surface heat flux loss over the southern part of the domain (Figure 4.1a) corresponds to the strong winds (strong southeasterly winds to the southeast and strong southerly winds to the

southwest of the model domain) as depicted in Figure 4.2a. The corresponding relatively cool SST in this region results from the net sea surface heat flux loss (mainly evaporation driven by the winds) (Figures 4.1b, c). The regions dominated by weak wind stresses such as that between 2^0S and 2^0N near the coast or that off the northwestern tip of Madagascar tend to have the net surface heat flux gain (about 50-80 Wm^{-2} and 10-50 Wm^{-2} respectively). This region of heat gain from the atmosphere off the northern Kenyan and Somali coasts may be related to the cold wedge, evident in March and April (and to lesser extent in May) (Figures 4.1b-c, q-r), that typically results from the bifurcation of the northward flow coming from the south and the formation of the Southern Gyre (Schott et al, 1990). The cold wedge results in a cooler ocean surface than the surrounding air leading to a greater net sea surface heat flux gain. The net sea surface flux gain then broadly contributes to increase of SST in May (Figures 4.1b-c).

By July, the South West monsoon is fully developed and the ITCZ is located over India (Gadgil, 2003). During this period, the SST in the western Indian Ocean and East African coastal waters appears to have cooled to about 26^0C while in the southeast of the study domain, a cooler SST tongue of about 24^0C exists near Cape Amber (Figures e, f). These values agree with Nyandwi et al. (2001) who observed that the SST off Tanzanian coast ranges from 25^0C to 26^0C in July. The strong south-easterly winds over the southeast of the model domain (east and north of Madagascar) (Figure 4.2b) match well with the net heat flux loss of about 50 to 100 Wm^{-2} (Figure 4.1d) and there is cooler SST due to the net heat flux loss. These strong south-easterly winds principally cool the SST through evaporation and upper-

ocean mixing. The relatively cool SST in the tropical western Indian Ocean is basically associated with the strong South West monsoon wind which is considered as a continuation across the equator of the Southeast Trades as portrayed in Figure 4.2b. The strong alongshore winds result in Ekman transport offshore north of equator and onshore south of the equator. Thus, upwelling occurs off Somalia near 4-5^{0}N and downwelling in the Tanzanian and southern Kenyan coastal waters. In the upwelling region, the ocean surface gets cooler than the surrounding air as a consequence there is a resultant net heat gain (50 to 100Wm^{-2}).

During September, towards the end of the South West monsoon, the coolest SST tongue (about 24^{0}C) extends from southeast to northwest of the model domain, towards the East African coast at about 8^{0}S and 10^{0}S (Figures 4.1h, i). This tongue corresponds with the strong south-easterly winds over the southeast of the model domain which are confined to south of 6^{0}S (Figure 4.2c). The strong south-easterly winds lead to ongoing upper ocean mixing and cool SST. The rest of the model domain is dominated by weak winds e.g. over the southwest, north of 6^{0}S and along the equator particularly its east (Figure 4.2c). These regions correspond with a net heat flux gain greater than 100Wm^{-2} (Figure 4.1g) resulting in relatively warm SST ranging from 26 to 27^{0}C in both model result and TMI-SST (Figures 4.1h, i).

During November, the transition or pre-onset of the North East monsoon, the spatial plot of the winds (Figure 4.2d) shows that there are strong south-easterly winds over the southeast of the model domain (north and east of Madagascar), north-easterly winds to the north of the model domain (an early development stage of the North East monsoon) and easterly winds from 46^{0}E towards the African coast. The strong

south-easterly winds over the southeast of the model domain correspond to the cool SST of about 26^0C (Figures 4.1k, l). This is due to evaporation and wind-induced upper ocean mixing and hence a low heat gain (less than 60Wm^{-2}) compared to the rest of the model domain in Figure 4.1j is evident. The regions with weak winds such as over the southwest, north and east of the model domain (Figure 4.2d) match with the significant net heat flux gain between 80 and 120 Wm^{-2} covering the whole domain except the far southeast and north (Figure 4.1j). Thus, the SST has increased to between 29^0C and 30^0C as observed in both datasets (Figures 4.1k, l). In the Tanzanian waters, the SST appears to be about 27.5^0C in November which agrees with UNEP (1985) and Mahongo (1999) who suggested a SST of about 27^0C in November. In general, this significant net heat flux gain in the whole domain can also be associated with the sun overhead of the Tanzanian region as it moves south of the equator in late September. Tomczak et al. (1994) stated that the ITCZ is about 4 to 6 weeks lagged behind by the sun. It can be deduced that the ITCZ moves over Tanzania from October to November. Thus, the Tanzanian and western tropical Indian Ocean are in general continually heated throughout from September to November resulting in a net surface heat flux greater than 100 Wm^{-2} by November.

During January, the peak of the North East monsoon, in both the model and satellite derived fields in Figures 4.1 n and o respectively; there is a distinct north-south gradient of SST with the southern section having warmer waters of about 29^0-30^0C and the northern section cooler waters of about 26^0-27^0C. These two zones are separated by a large temperature gradient which is associated with horizontal circulation and contributes to heat advection towards the cooler zone. Over the

region between 4^0S and 5^0N, a zone of cool waters is marked by the strong northeasterly winds (Figure 4.2e) resulting in a large temperature difference between surface ocean and the surrounding air. As a consequence, a net heat gain of 50 to 80 Wm^{-2} is evident there (Figure 4.1m). The region of net heat gain corresponds well to that of relatively cool SST. The low net heat flux gain further north in the model domain can be associated with the forcing beyond the domain of the study. A zonal tongue of warm SST between 4^0S and 10^0S is marked by weak northeasterly winds (Figure 4.2e). As a consequence, there is a low net heat gain, less than 50 Wm^{-2}, as shown in Figure 4.1m due to the small temperature difference between the ocean surface and the overlying air. However, in the south of the model domain (south of 10^0S), there are very weak southeasterly winds which correspond to the net sea surface heat flux gain of between 40 and 80 Wm^{-2} and a corresponding rise of SST is evident in both datasets (Figures 4.1n, o).

During March when the North East monsoon comes to an end, the model SST seems to be somewhat greater than the satellite data as shown in figures 4.1r and s. But in both datasets, there is a distinct north-south gradient of SST with the northern section (north of 4^0S and 5^0S in the model and TMI results respectively) having a relatively cool SST of about 27^0-28.5^0C and the southern section (south of 4^0S and 5^0S in the model and TMI results respectively) having warmer waters with SST ranging between 28.5^0C and 31^0C. The warmest SST of about 29.6^0C is apparent east of the Tanzanian coastal ocean, near 10^0S where Rao et al. (2005) found SST values of about 29^0C in March. These observations tend to agree with Julius (2005) and Newell (1959) who stated that there is maximum SST ranging from 28^0C to 30^0C

in March and April. As the North East monsoon dies down during March, the winds near Tanzania are fairly similar to those found in November as portrayed in Figure 4.2f. The relatively cool SST in the north of the model domain is associated with the strong northeasterly and easterly winds and hence a corresponding increase of the net heat flux gain, greater than 100 Wm^{-2} between 5^0S and 5^0N (Figure 4.1p). Except to the east of Madagascar, the rest of the region south of 5^0S has weak winds blowing in different directions and, as a consequence, very weak evaporation and upper ocean mixing occur, thus resulting in a corresponding low net heat gain of about 50 to 70 Wm^{-2} (Figure 4.1p). In late March, the sun is overhead over Tanzania when it moves northward and this possibly contributes to the net heat flux gain due to high short wave radiation gained from the sun north of 5^0S.

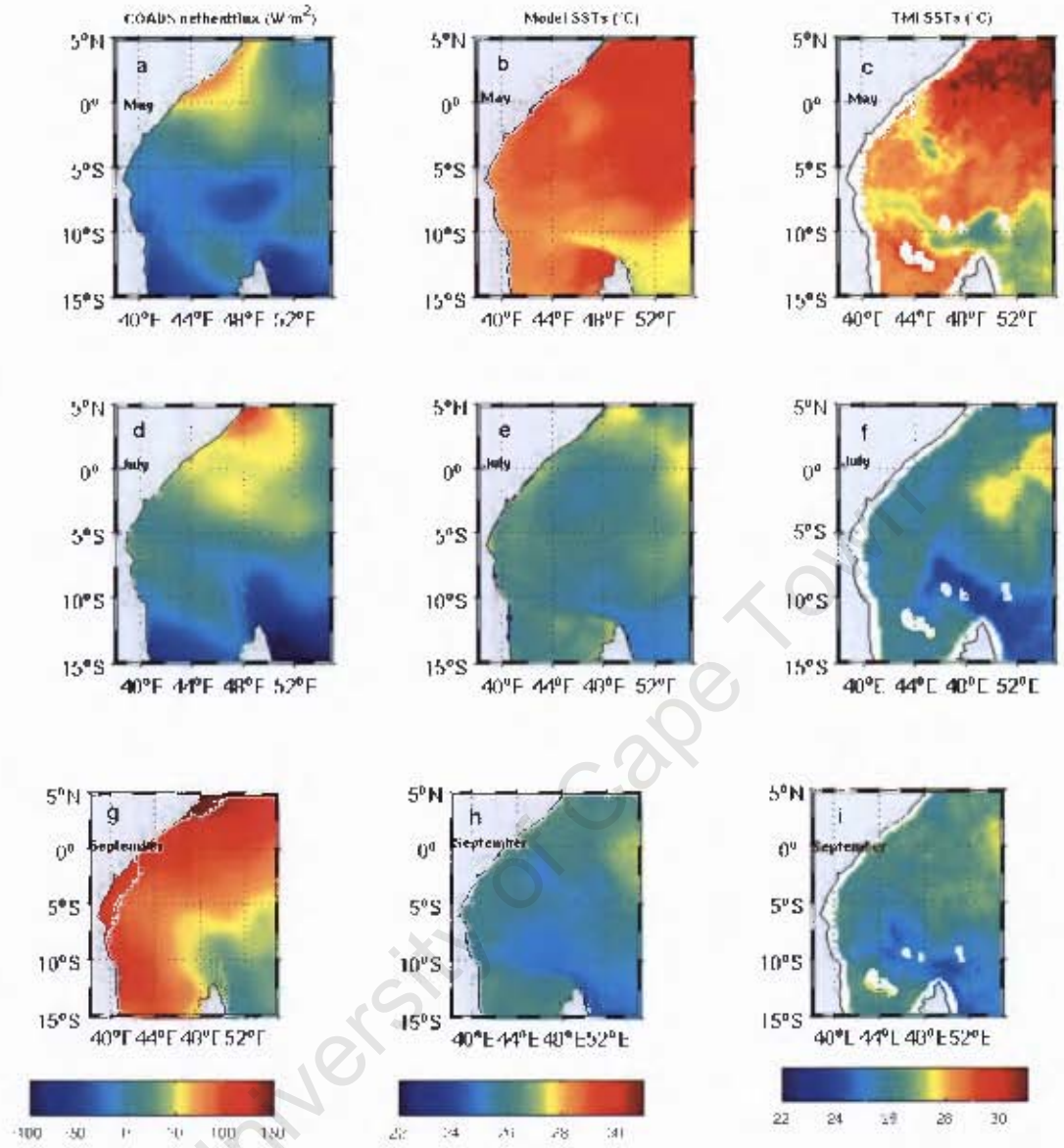

Figure 4.1a-i: The properties of the East African coastal ocean for May (panels a, b and c), July (panels d, e and f), September (panels g, h and i) showing model net surface heat flux in column one, model SST in column two and satellite derived (TMI) SST in column three. Note that there is about 50km data gap along the coastal zone in the TMI-SSTs attributed to contamination of satellite radiometer by continental or island landmasses.

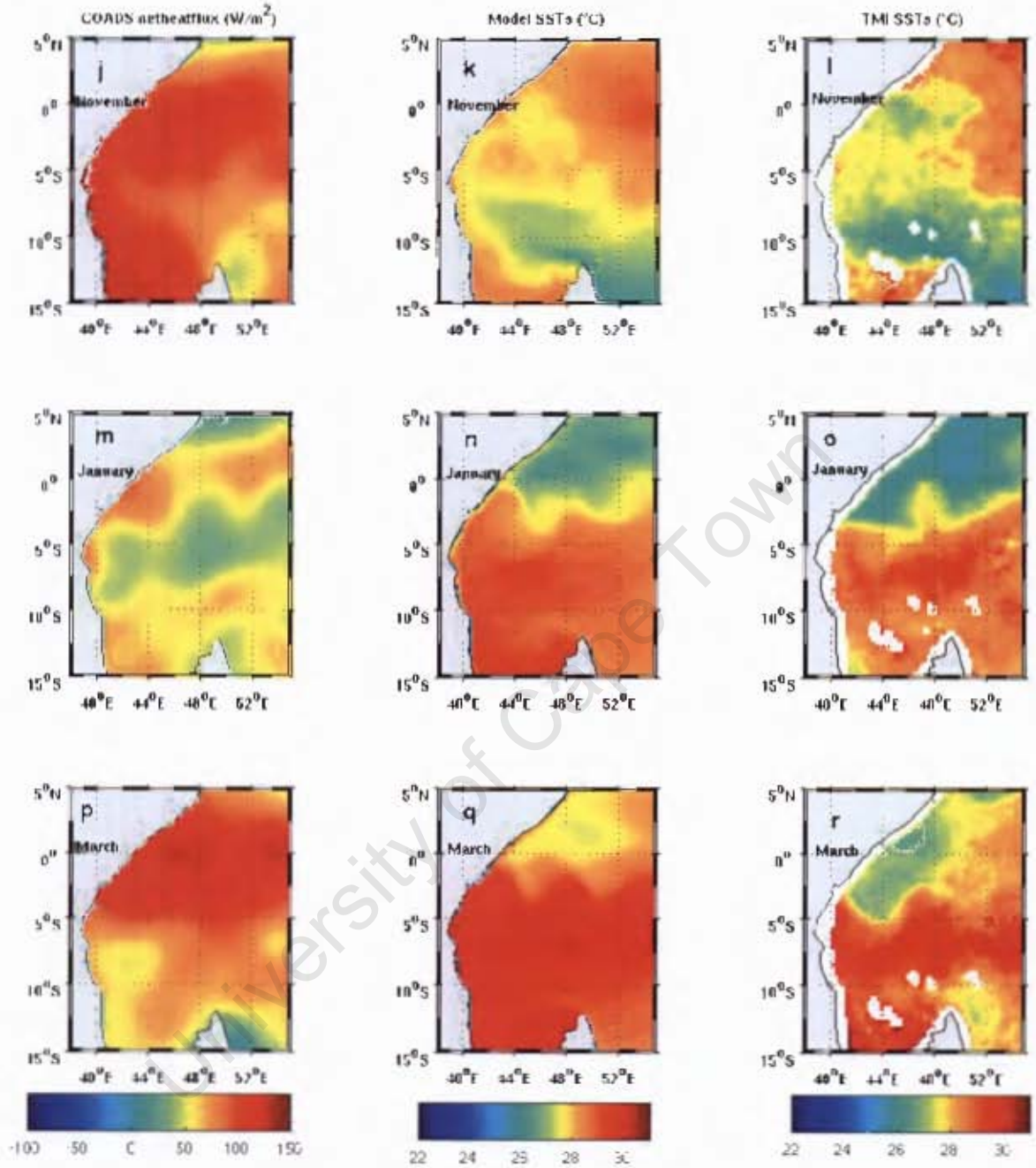

Figure 4.1j-r: The same as figure 4.1a-i but for November (panels j, k and l), January (panels m, n and o) and March (panels p, q and r)

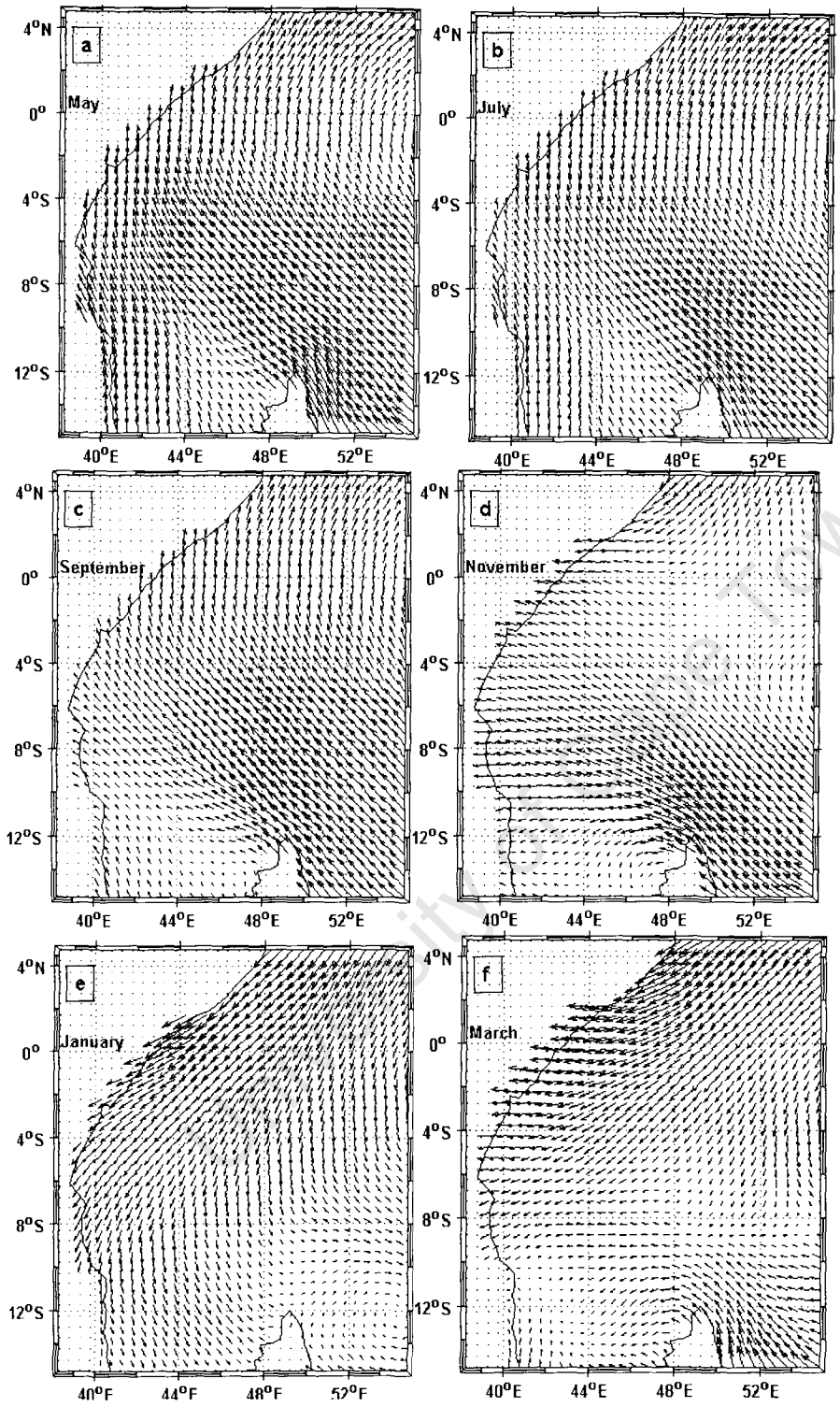

Figure 4.2: COADS wind stress field in Nm^{-2} over the East African coastal ocean for May (a), July (b), September (c), November (d), January (e) and March (f).

4.2 The East African Coastal Current (EACC)

The model output of the East African Coastal Current speeds are portrayed in Table 4.1 and Figure 4.3. Single point time series of the EACC speeds and their corresponding meridional wind stresses from 10^0S, 8^0S, 6^0S, 4^0S and 2^0S between 40^0E and 42^0E (Figure 4.4), off the coast of East Africa indicate the spatial and temporal variations. These time series of the EACC speeds and their corresponding meridional wind stresses have positive correlation coefficients (r) greater than 0.6 (i.e. 0.69 at 10^0S, 0.89 at 8^0S, 0.74 at 6^0S, 0.70 at 4^0S and 0.64 at 2^0S). However, they have very small p-values, less than 0.05 (i.e. 0.001 at 8^0S which shows a true correlation, 0.03 at 2^0S and 0.01 at 4^0S, 6^0S and 10^0S) and hence they are statistically significant. Thereby, the strength of the EACC is greatly determined by the meridional wind stresses over the East African Ocean.

During the North East monsoon (December-March), the EACC is weaker than the rest of the year, meeting with the Somali Current between 1^0S and 2^0S. In December, the EACC appears to interact with a very weak southward Somali Current near 1^0S and turns off the coast to form the SECC (Figure 4.3l). The model result in this month show prominent eddies that are trapped by the SECC possibly result from the Northern Equatorial Current near 3^0N that feeds into the eddy. In January, the speeds of the EACC are weaker than in December in all locations but gradually increase northwards (Table 4.1, Figures 4.3a and 4.4). The EACC appears to have speeds of about $1ms^{-1}$ between 1^0S and 5^0S and less than $0.65ms^{-1}$ between 5^0S and 10^0S. The confluence zone (about 1^0S) and eddies in December also occur in January with a weak turning-off the coast to an eastward flow with

eddies. The lowest speed of the EACC is apparent in the month of February when the confluence zone is located at about 2^0S (Figure 4.3b). In this month, the EACC appears to have speeds less than 0.9ms^{-1} with speeds of about 0.88ms^{-1} at 4^0S; 0.62ms^{-1} at 2^0S, 6^0S and 8^0S; and about 0.38ms^{-1} at 10^0S (Figures 4.3b, 4.4a-e, Table 4.1). By March, the EACC strengthens with speeds of about 1.15ms^{-1} and 1.2ms^{-1} apparent at 4^0S and 2^0S respectively; and 0.88ms^{-1}, 0.65ms^{-1} and 0.35ms^{-1} at 6^0S, 8^0S and 10^0S respectively. The confluence zone is located at about 1^0S as in December and January (Figure 4.3c). The model results demonstrate the confluence zone well, which varies from 1^0S to 2^0S in December to March. The location of the confluence zone ranges from 1^0N at the beginning of the winter season to 4^0S during the February peak, when the EACC is at its weakest as suggested by Tomczak et al. (1994). Thus, the northern limit of the model EACC is reasonably considered to be at about 2^0S rather than 3^0S as suggested by Swallow et al. (1991) and at the equator by Newell (1957) due to its confluence zone with Somali Current occurring from 1^0S to 2^0S in North East monsoon (Figures 4.3a, b, c, l). The variability of the EACC during these months, December to March can be associated with the strength of the southward meridional wind stresses. These meridional wind stresses increase northward from December to March when the South West monsoon fades while the North East monsoon is in early stages of development; and they correspond to the spatial and temporal increase of the EACC speeds northwards (Figure 4.4, Table 4.1). The strong southward meridional wind stresses that occur in January to February off the East African coast (Figure 4.4) provide strong resistance to the EACC resulting in the lowest speeds in February (Figure 4.3b and 4.4). Tomczak et al. (1994) suggested that the EACC shows its weakest speed in February consistent

with the model results. Furthermore, the EACC tends to be turning offshore towards the open ocean (Figures 4.3a, b, c, l) during the North East monsoon which can be associated with the confluence mechanism between the EACC and Somali Current.

The situation is different during the pre-monsoon, South West monsoon and post-monsoon seasons from April to May; June to September; and October to November when there are northward meridional wind stresses along the EACC, offshore from the coast of East Africa (Figure 4.4). In the transition months of the pre-monsoon (April and May), the EACC appears to have nearly similar speeds as depicted on the Figures 4.3d, e, 4.4 and Table 4.1. The spatial distribution of the average speeds of the EACC derived from the model results (Table 4.1) for April and May are about $0.58ms^{-1}$ at 10^0S, $0.86ms^{-1}$ at 8^0S, $1.20ms^{-1}$ at 6^0S, $1.45ms^{-1}$ at 4^0S, $1.35ms^{-1}$ at 2^0S. The model again shows the confluence zone suggested by Tomczak et al. (1994) which reaches the equator in early April and then moves north (Figure 4.3d). In May, the Southern Gyre is apparent in the model results when the extension of the EACC, the Somali Current, crosses the equator and one part of it turns offshore at 2^0N. These observations are attributed to the small difference in the northward meridional wind stresses along the EACC in these two months (Figure 4.4) and correspond to the speeds of the current as shown in Figure 4.3d, e. The flow offshore of the southern Tanzanian coast (at 10^0S) and at 2^0S show great variability in speeds probably due to effect of the NEMC which depends on the southeasterly winds and the monsoonal changes north of and near the equator respectively.

During the South West monsoon (June to September), the EACC becomes stronger than the other months of the year; with the greatest speed of about 1.65 ms^{-1} during

July (Table 4.1, Figures 4.4 and 4.3f, g, h, i). The monthly average speeds extracted from Table 4.1 from June to September are as follows: 0.65 ms^{-1} at 10^0S, 0.92 ms^{-1} at 8^0S, 0.98 ms^{-1} at 6^0S, 1.4 ms^{-1} at 4^0S and 1.53 ms^{-1} at 2^0S. In these months, the South West monsoon wind is fully developed and helps to drive the East African Coastal Current (Julius, 2005; Dubi, 2000; Newell, 1957) as shown by the presence of strong northward meridional wind stresses (Figure 4.4). The minimum speed in these months is about 0.6ms^{-1} at 10^0S in September when the South West monsoon is fading, and it appears to increase northwards to 4^0S (Figures 4.3d-g, 4.4a-d, Table 4.1). The strongest speeds of the EACC in June and July (particularly for 2^0S-6^0S) are attributed to the presence of the strong northward meridional wind stresses which support the EACC (Figure 4.4). The northward meridional wind stresses gradually decrease from the peak of the South West monsoon (July) to September when the South West monsoon fades (Figure 4.4) and hence weakly support the EACC that results in gradual decrease of speeds (Figures 4.3h, I, 4.4, Table 4.1).

During the post-monsoon or transition season, October to November, the EACC shows speeds greater than 1ms^{-1} from 6^0S northwards as also happens in pre-monsoonal months (April and May) (Figures 4.3d, e, j, k, 4.4, Table 4.1). The average monthly speeds of the EACC deduced from Table 4.1 for October and November show the speeds of about 0.4 ms^{-1} at 10^0S, 0.72 ms^{-1} at 8^0S, 1.05 ms^{-1} at 6^0S, 1.43 ms^{-1} at 4^0S and 1.51 ms^{-1} at 2^0S. The decrease of the EACC speeds can be associated with the further decrease of the meridional wind stresses in October to November when the North East monsoon is in its early development stage (Figure 4.4). The lowest speed occurs at 10^0S in November and is about 0.3ms^{-1}. A similar

value occurs March which is due to nearly equal meridional wind stresses in March and November (Figures 4.4a, Table 4.1). The meridional wind stresses in March and November appear to be zero as they change direction from southward to northward in March and the reverse in November (Figure 4.4). Nevertheless, the EACC speeds during these months at 8^0S are nearly equal (Figure 4.4, Table 4.1). In general, there is a rapid increase of the monthly mean speeds northward of the surface current in April and through the northern summer. Subsequently, speeds decrease slowly through the rest of the year as also found by Swallow et al. (1991) (Table 4.1).

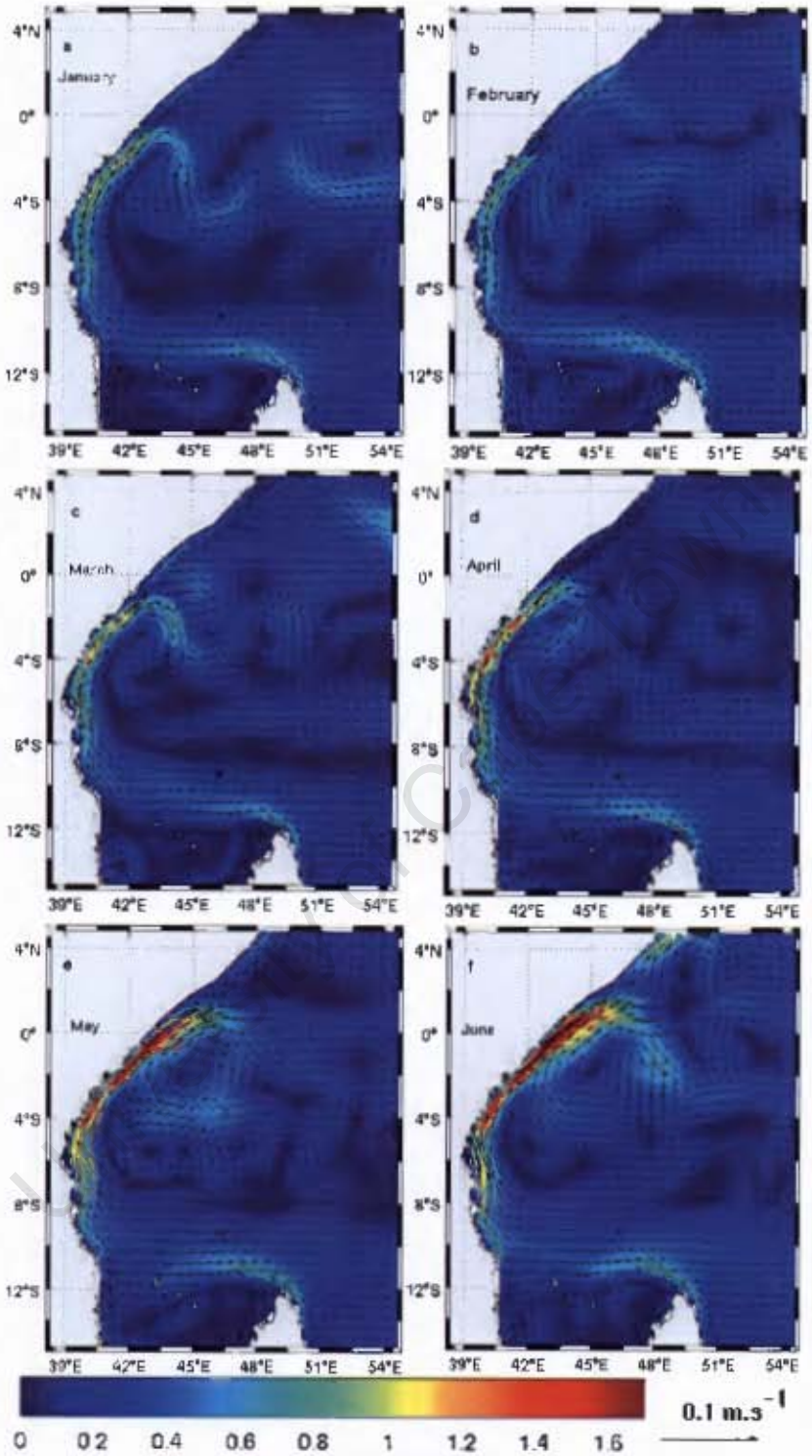

Figure 4.3 (a-f): The East African Coastal Current (EACC) speeds (ms $^{-1}$) from January to June.

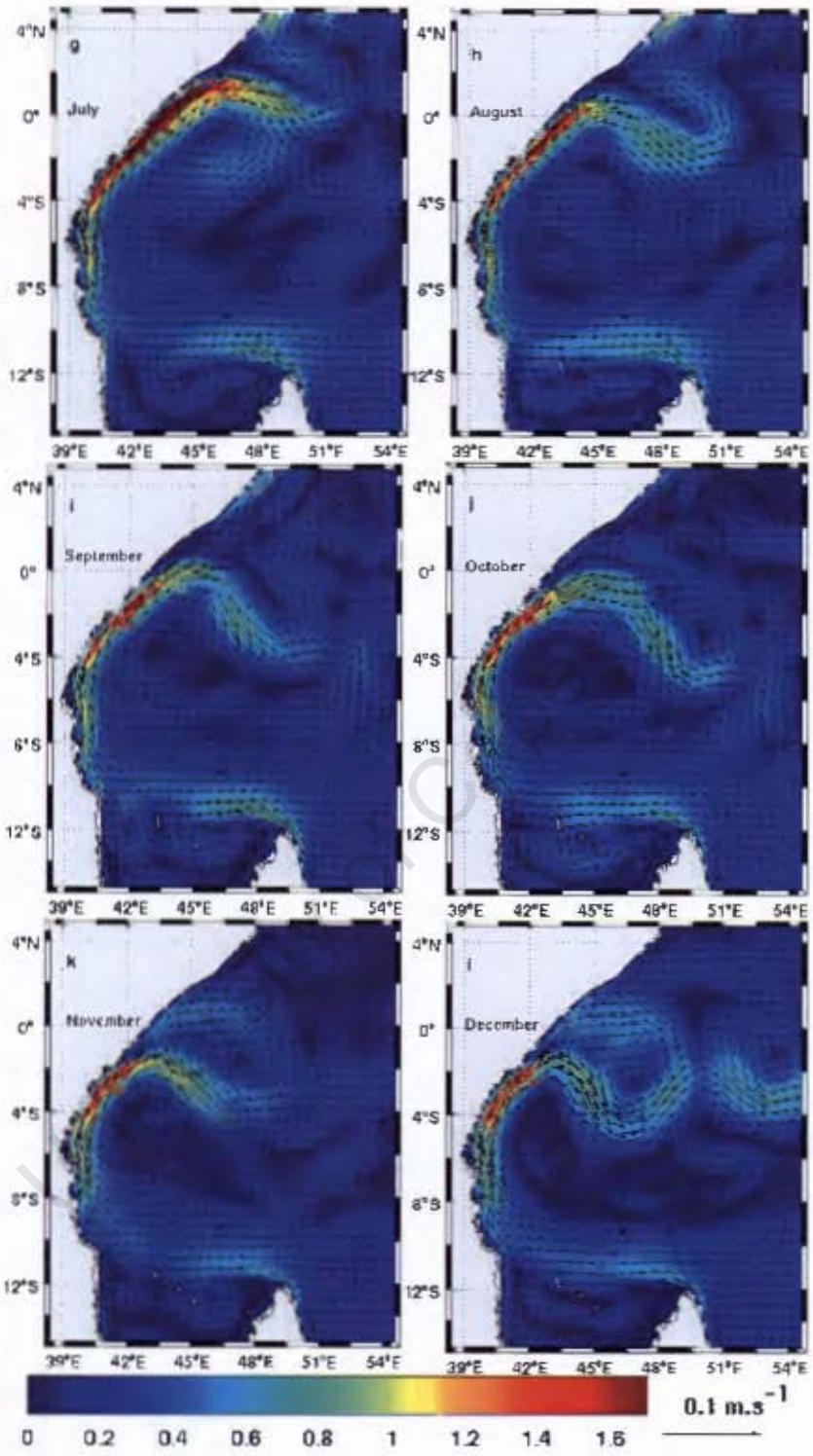

Figure 4.3 (g-l): The East African Coastal Current (EACC) speeds (ms^{-1}) from July to December

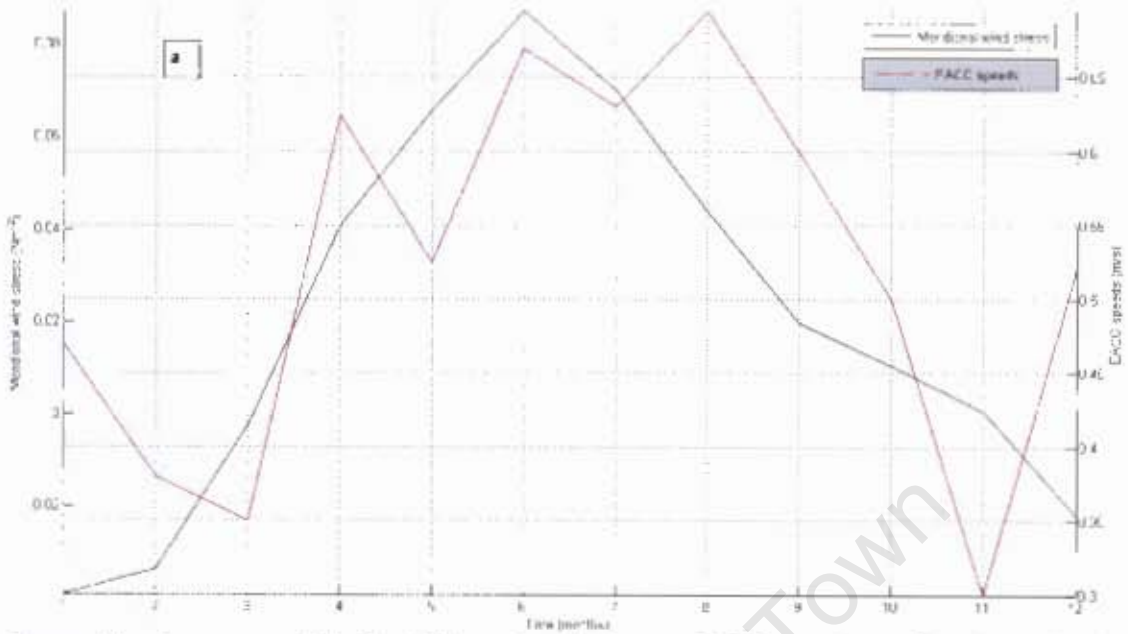

Figure 4.4a: Time series of the East African Coastal Current (EACC) speeds (ms^{-1}) and meridional wind stresses (Nm^{-2}). A correlation coefficient r =0.69 and p=0.01 was computed between these two variables at 10^{0}S and between 40^{0} and 42^{0}E off coast of East Africa.

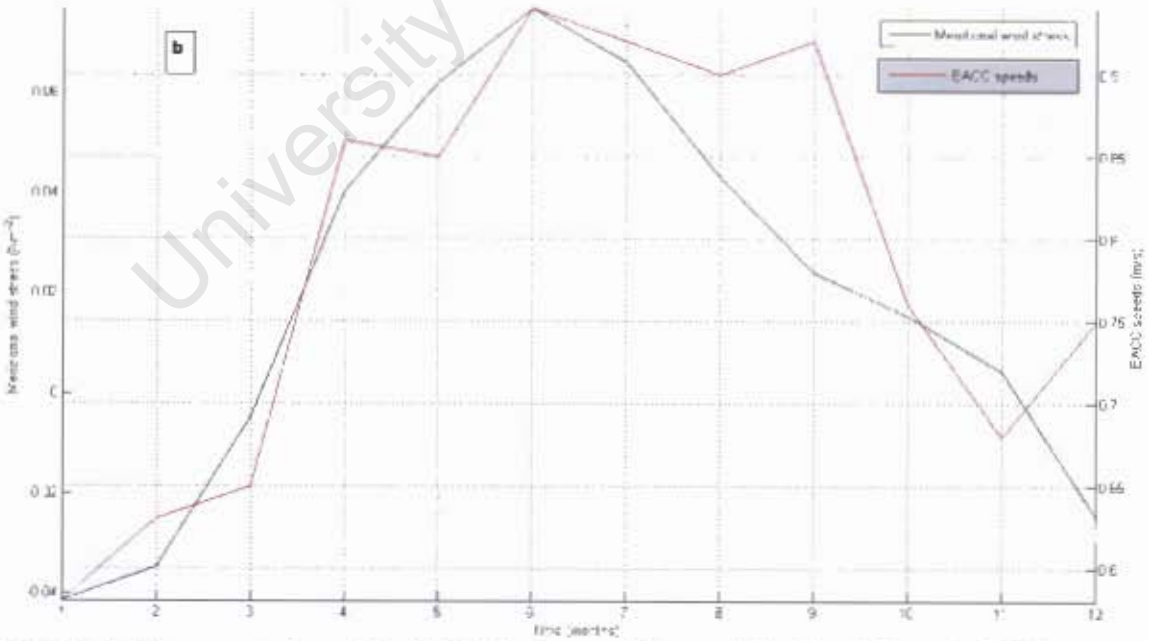

Figure 4.4b: The same as figure 4.4a at 8^{0}S with the correlation coefficient (r) =0.89 and p=0.001

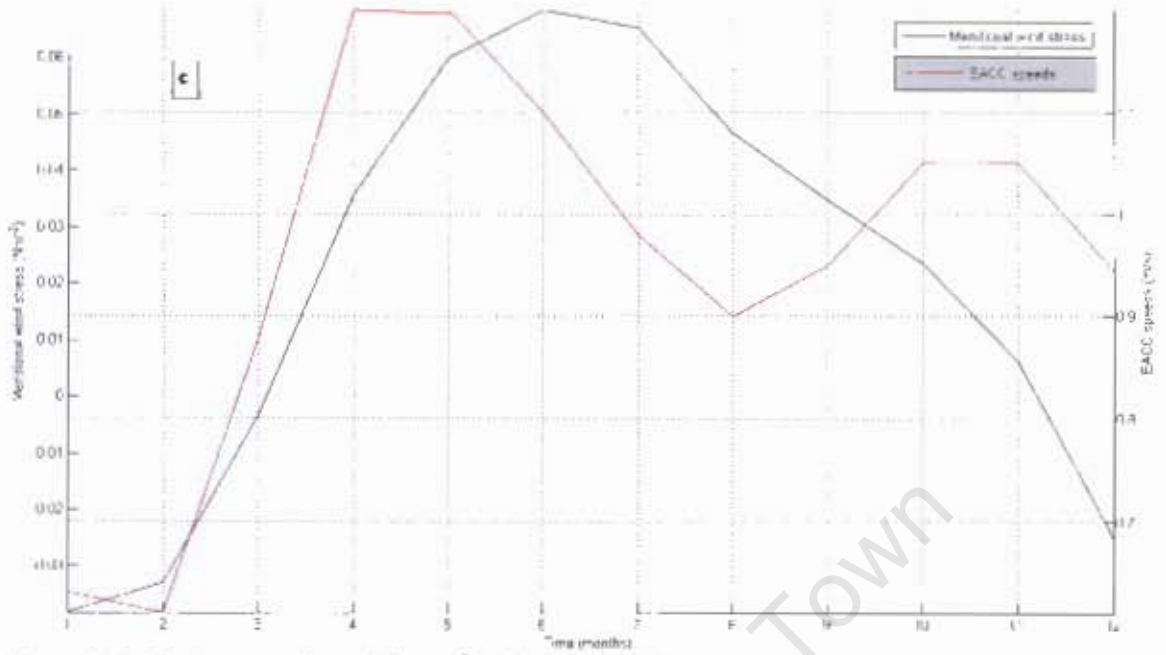

Figure 4.4c: The same as figure 4.4a at 6°S with the correlation coefficient (r) =0.74 and p=0.01

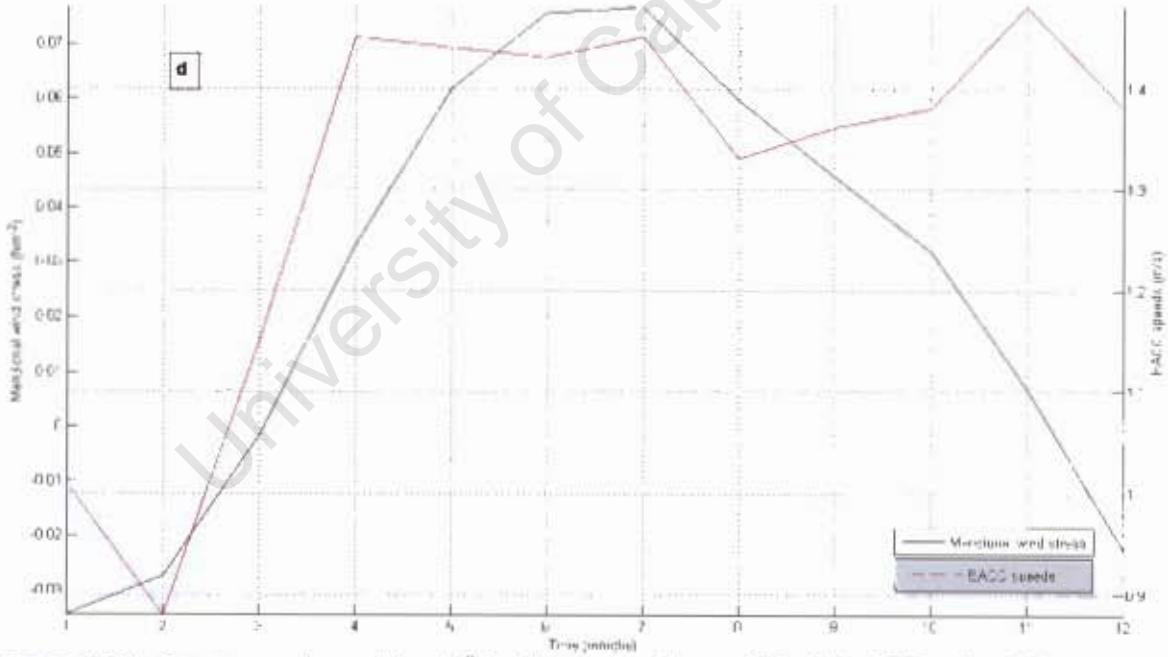

Figure 4.4d: The same as figure 4.4a at 4°S with the correlation coefficient (r) =0.70 and p=0.01

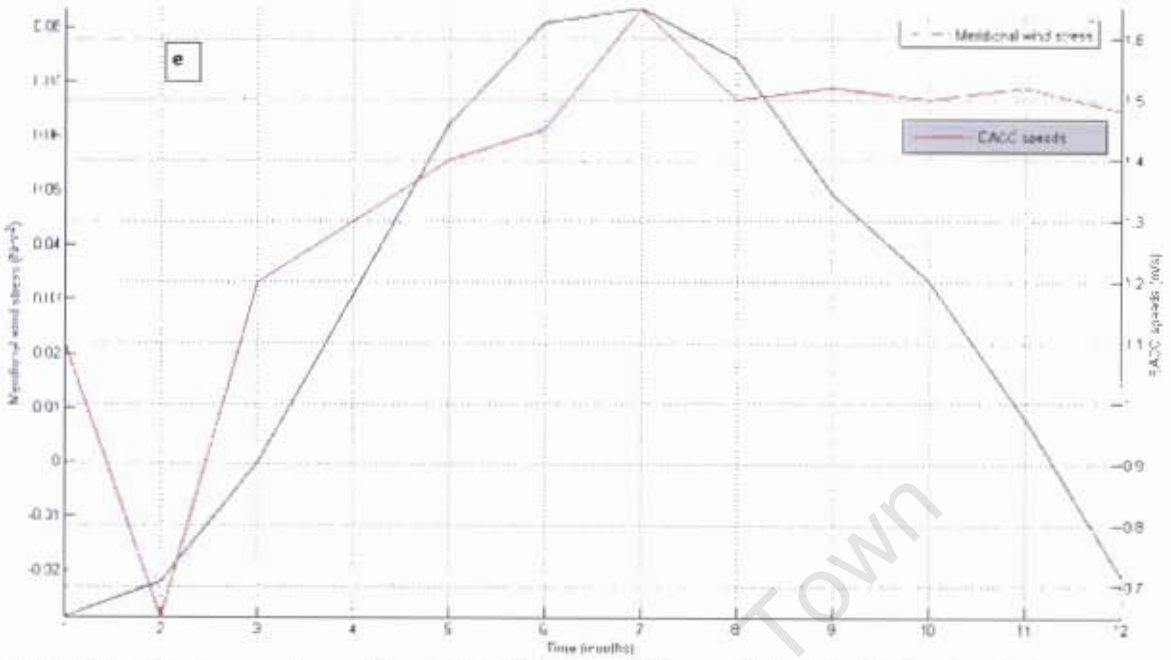

Figure 4.4e: The same as figure 4.4a at 2°S with the correlation coefficient (r) −0.64 and p=0.03.

Table 4.1: The monthly mean speeds (ms^{-1}) of the East African Coastal Current (EACC) derived from the model time series Figures 4.2a e.

Latitude	Jan	Feb	Mar	Apr	May	Jun	Jul	Aug	Sep	Oct	Nov	Dec
10°S	0.47	0.38	0.35	0.63	0.53	0.67	0.63	0.7	0.6	0.5	0.3	0.52
8°S	0.58	0.63	0.65	0.86	0.85	0.94	0.92	0.9	0.92	0.76	0.68	0.75
6°S	0.63	0.61	0.88	1.20	1.20	1.10	0.98	0.9	0.95	1.05	1.05	0.95
4°S	1.01	0.88	1.15	1.45	1.44	1.43	1.45	1.33	1.36	1.38	1.48	1.38
2°S	1.1	0.65	1.2	1.3	1.4	1.45	1.65	1.5	1.52	1.5	1.52	1.48

4.3 The relationship between the annual cycle of the flow entering the coastal ocean off southern Tanzania and the seasonality north of Madagascar

The comparison of the point time series of the NEMC speeds for the flow to the north of Madagascar and the EACC in the coastal ocean off southern Tanzania is shown in figure 4.5. The NEMC which flows northwestwards past Cape Amber, shows an average annual surface speed of 0.68 ms^{-1} which is nearly equal to that argued by Schott et al. (2001) of about 0.7ms^{-1} with annual speed range of about 0.15ms^{-1}. The maximum speed of the flow of about 0.78ms^{-1} to the north of Madagascar occurs in September when the South West monsoon fades and minimum speed occurs in November, the transition period to the North East monsoon. The annual surface flow in the coastal ocean off southern Tanzania is about 0.52ms^{-1} with an annual speed range of about 0.4ms^{-1}. The maximum speed flow of about 0.7ms^{-1} occurs off the southern Tanzanian coast in August when the South West monsoon is fully developed and minimum speed flow of about 0.3ms^{-1} occurs in November as to the north of Madagascar. The annual speed ranges show that there is a greater monthly variability in the southern Tanzanian flow than that north of Madagascar due to the strong influence of the meridional wind stresses. This can be verified by the correlation coefficient (r) between the EACC and their corresponding meridional wind stresses of about 0.69 and $p=0.01$ while that of the NEMC in northern Madagascar is about 0.51 and $p=0.09$ (Figures 4.4a, 4.6). The p-value of the coastal ocean flow off southern Tanzania ($p<0.05$) shows that the meridional wind stresses and flow are statistically significant while that north of Madagascar are not ($p>0.05$). The strength of the correlation between the coastal ocean flow off southern Tanzania

and that of northern Madagascar is r =0.57 and p=0.05 and hence they are slight statistically significant (Figure 4.5).

During January to March (JFM), both the coastal ocean flow off southern Tanzania (EACC) and that north of Madagascar (NEMC) gradually decrease from 0.47ms^{-1} in January to 0.35ms^{-1} in March and from 0.70ms^{-1} in January to 0.64ms^{-1} in March respectively. This is the time when there are north-easterly winds over the Indian Ocean between 12^{0}S and equator (Hermes and Reason; 2008) which includes the Tanzanian coastal ocean. The north-easterly winds blow against the EACC in the southern Tanzanian coastal ocean as shown by the presence of strong southward meridional wind stresses (Figure 4.4a). Over northern Madagascar, the south-easterly winds located to the south of 10^{0}S persist throughout the year (Tomczak et al, 1994) and merely weaken during the North East monsoon. As a consequence, these winds weakly support the NEMC. The gradual decrease of the flow speeds correspond to the weak meridional wind stresses to the north of Madagascar during January to March (Figure 4.6).

During the pre-South West monsoon season (April and May), there is a sharp increase in the speed of the flow off the southern Tanzanian coast to about 0.63ms^{-1} in April with a subsequent decrease of the speed to about 0.53ms^{-1} in May. The speeds to the north of Madagascar appear to increase gradually from 0.70ms^{-1} in April to 0.73ms^{-1} in May. This is the time when the Tanzanian waters experience a transition from the north-easterly winds into south-westerly winds which results in abrupt speed changes in April and May. During April to May, the south-easterly

winds continually strengthen; hence there is a gradual increase in the speeds of the flow to the north of Madagascar from April to May (Figure 4.6).

During the South West monsoon (June to September), the speeds of both flows decrease from 0.67ms^{-1} in June to 0.63ms^{-1} in July for the flow off the southern Tanzanian coast and from 0.72ms^{-1} in June to 0.71ms^{-1} in July for the flow to the north of Madagascar. Further decreases occur in the flow north of Madagascar in August. These decreases can be associated with the strong meridional wind stresses (Figure 4.6) that poorly support the northwest flow in the north of Madagascar. The south-easterly winds tend to be the strongest and extend further north during this season (Tomczak et al, 1994). There are high speeds of the flow off the southern Tanzanian coast with a maximum speed in August when the south-westerly wind is fully developed and supports the EACC. The maximum speed to the north of Madagascar occurs in September when the south-westerly winds between 12^{0}S and the equator fade and the decrease of the meridional wind stresses in Figure 4.6 is evident.

In October and November, the transition period to North East monsoon, there is a sharp decrease in the speeds of the off flow to both the southern Tanzanian coast and north of Madagascar from 0.5ms^{-1} in October to 0.3ms^{-1} in November and from 0.66ms^{-1} in October to 0.63ms^{-1} in November respectively. This change is similar to that for the pre-South West monsoon season in April and May for the flow off the southern Tanzanian coast which seems to be more affected by the monsoon winds than that to the north of Madagascar. Both flows appear to have their minimum speeds in November. Thereafter, they continue to increase in December (the

beginning of the North East monsoon) when the speed increases to 0.5ms^{-1} off the southern Tanzania coast and 0.64ms^{-1} to the north of Madagascar. In general, the flow in the southern Tanzanian coastal ocean is mostly influenced by the south-easterly and north-westerly wind reversal which occurs between 12°S and the equator in austral winter and summer respectively.

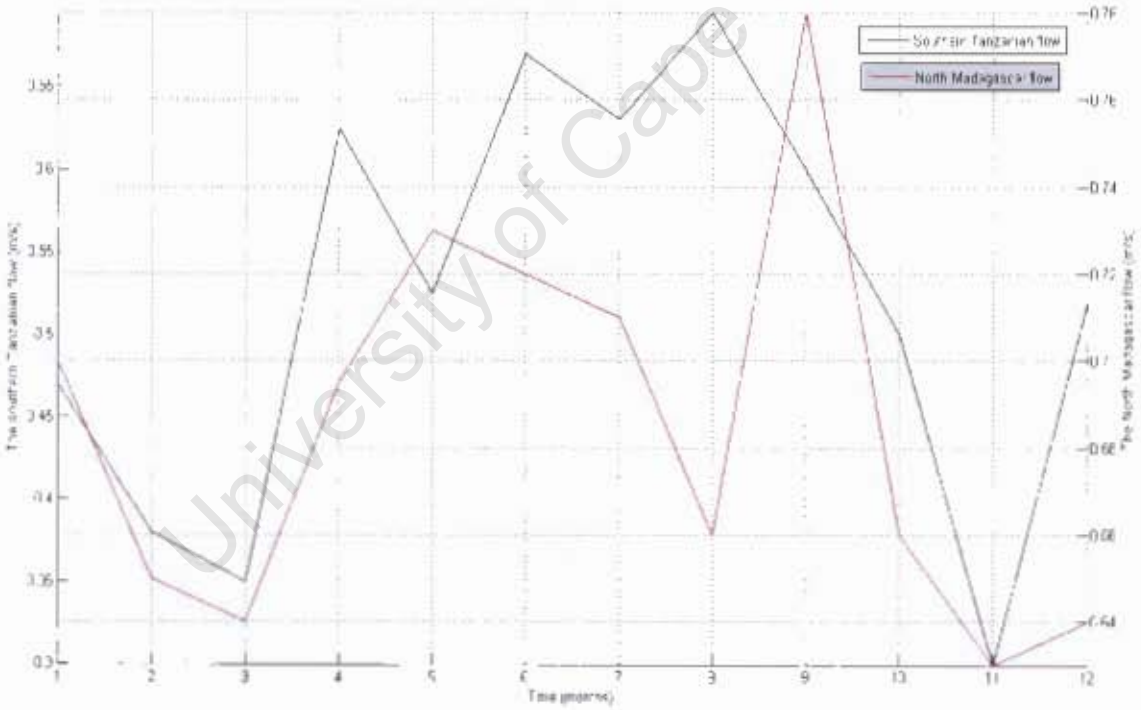

Figure.4.5: The time series of the mean speeds (ms^{-1}) of the EACC and NEMC in the southern Tanzanian coastal ocean (10°S, 40-42°E) and the NEMC the north of Madagascar (11.8°S, 49°E) respectively. A correlation coefficient r =0.57 and p=0.05 is computed between these two variables.

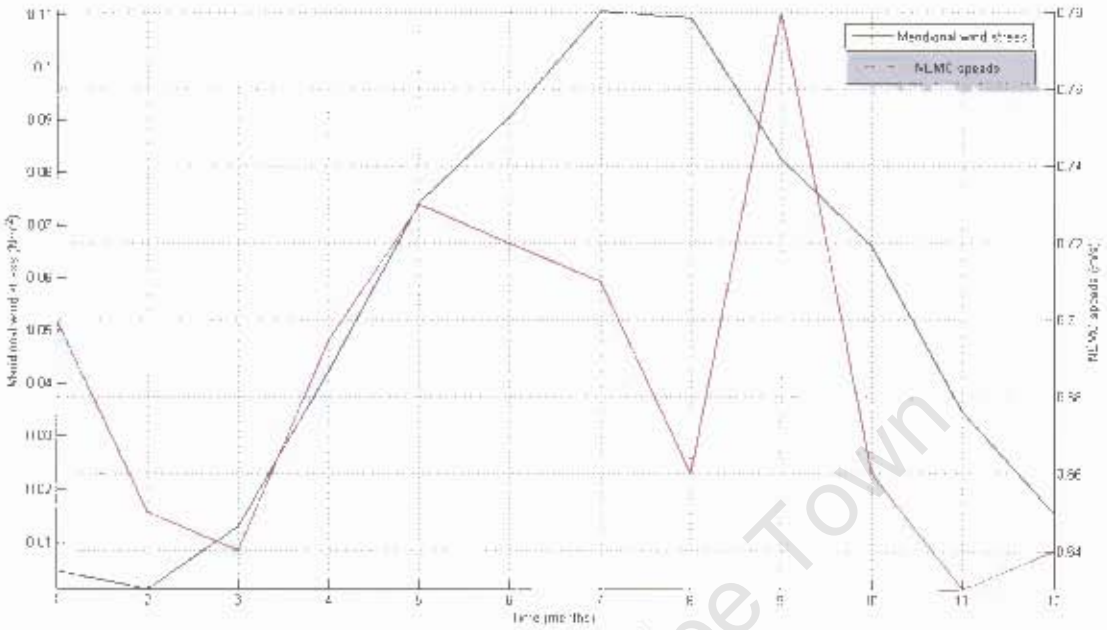

Figure 4.6: The time series of the mean speeds (ms^{-1}) of the NEMC and the meridional wind stresses (Nm^{-2}) to the north of Madagascar at 11.8^0S and 49^0E. A correlation coefficient r =0.51 and p=0.09 is computed between these two variables.

4.5 Summary

The results and discussion chapter deals with the ten years model simulation output of ROMS model experiment that was forced by a monthly climatology of the wind stresses and heat fluxes derived from individual observations in COADS from January, 1945 to December, 1989. The model output of the annual cycle of the sea surface temperature was compared with the satellite derived TMI-SST measurements for the same region. In general, the model SSTs were warmer than the TMI satellite derived observations. However, it must be noted that the two datasets are not strictly comparable. For example, the model has been forced with COADS data corresponding to a period from 1945-1989 climatology whereas the

satellite SST corresponds to a 2000-2004 climatology, years with very little or no effects from the ENSO and IODZM. Also, the satellite data is a microwave imager (can see through clouds) whereas the COADS data is mainly based on *in situ* ship observations.

The chapter contains three sections which are based on the research questions of this dissertation, namely Annual cycle of the sea surface temperature and net heat flux; the East African Coastal Current (EACC) and the relationship between the annual cycle of the flow entering the coastal ocean off southern Tanzania and the seasonality north of Madagascar.

The first section highlighted the annual cycle of the sea surface temperature and net heat flux over the Tanzanian continental shelf and its adjacent ocean associated with the wind stresses. By May, the cool zone appears to the southeast of the model domain which corresponds with the strong south-easterly winds and the net heat flux loss indicating strong cooling of the upper ocean. The Tanzanian coastal ocean and the rest of the model domain show warm SST of about 28-31^{0}C which is associated with weak winds over the region. In July to September, there is a relatively cool SST of about 25^{0}C to 27^{0}C in the tropical western Indian Ocean which is basically associated with the strong south-westerly winds, a continuation across the equator of the Southeast trades. In November, the pre-North East monsoon season, the western tropical Indian Ocean have temperatures ranging from 27-30^{0}C in both model and satellite derived data with winds blowing in different directions. By January, there is a distinct spatial (north-south) distribution of SST with the southern section (including the Tanzanian coastal ocean) having warmer waters about 29^0-

30^0C and the northern section showing cooler waters of about 26-27^0C. A zone of warm waters with SST that range between 28.5^0C and 31^0C extends further north to the equator by March.

The second section investigated the East African Coastal Current (EACC). This current appears to be mainly affected by the reversal of the winds over the Indian Ocean with both spatial and temporal variations of the speeds. There is a strong positive correlation between the EACC speeds and their corresponding meridional wind stresses in all locations (about $r>0.6$ and $p<0.05$). As a result, there is strong influence of the meridional wind stresses on the speeds of the EACC at locations off the East African coast at approximately 40^0E to 42^0E. The EACC appears to have speeds less than $0.9ms^{-1}$ in February which is considered as the month with its weakest speeds while the maximum speed of about 1.65 ms^{-1} is apparent during July in north at 2^0S, between 40^0E and 42^0E. During both transition seasons (April/May and October/November), the EACC shows speeds greater than $1ms^{-1}$ north of 6^0S. During the North East monsoon (December-March), the EACC appears to be weaker than the rest of the year, meeting with Somali Current between 1^0S and 2^0S.

The third and last section was concerned with the relationship between the annual cycle of the flow entering the southern Tanzanian coastal ocean and the seasonality north of Madagascar. The speeds of the flow off the southern Tanzanian coast and that north of Madagascar increase and decrease simultaneously during October to April with both attaining the lowest speeds in November. The flow speeds off the southern Tanzanian coast decrease from April to May and subsequently increase in

June while that to the north of Madagascar do the opposite of that off the southern Tanzanian coast. From June to July, the speeds of the flow in both places decrease followed by a further decrease by August to the north of Madagascar which can be associated with strong meridional wind stresses that do not support the north-westward current (NEMC). This can be observed clearly in figure 4.6 whereas the p-value is greater than 0.05 as a result; the meridional wind stresses and the NEMC are not statistically significant. The flow off the southern Tanzanian coast attains its maximum speed in August when the South West monsoon is fully developed and supports the EACC. The flow north of Madagascar attains its maximum speed in September when the South West monsoon fades. The flow off the southern Tanzanian coast and that to the north of Madagascar are positively correlated whereby r =0.57 and p=0.05. Thereby, as the Northern Madagascar flow increases, the flow off the southern Tanzanian coast increases and vice versa.

Chapter 5 Conclusion and Recommendations

This chapter deals with the conclusion of the regional model study of the numerical modelling of the East African coastal ocean (Tanzanian continental shelf waters and the adjacent ocean). The previous studies of the ocean dynamics and properties of the coastal ocean off Tanzania (Tanzanian continental shelf waters and the adjacent ocean) have shown that they are influenced by the monsoon, the large scale western and equatorial Indian Ocean circulation; the El Niño-Southern Oscillation (ENSO) and the Indian Ocean Dipole-Zonal Mode (IODZM) climate modes. The model study in this dissertation was conducted by running a model experiment with the **R**egional **O**ceanic **M**odeling **S**ystem **(ROMS).** The ROMS is the numerical code developed at Rutgers University and at the University of California, Los Angeles in USA as an improvement of S-Coordinates Rutgers University Model (SCRUM). It was forced with the COADS surface marine monthly climatological datasets for the period of 1945 to 1989. The MATLAB computing programming language and roms-graphical user interface (roms-gui) were used to analyse and display time series and spatial plots of the model results. The model study was aimed to investigate the annual cycle of the SST, the variability of the EACC in the transition seasons and the annual cycle of the flow entering the southern part of Tanzanian waters in relation to the seasonality north of Madagascar.

The sea surface temperature from the model results was compared to that of the Tropical Rainfall Measuring Mission (**TRMM**) Microwave Imager (**TMI**) satellite for the same region. These datasets appeared to match each other although the model SST output seemed to be warmer than satellite derived TMI data probably due to the

TMI-SST data being extracted from 2000 to 2004, years with very little or no effects from the ENSO and IODZM while the model was forced by wind stresses and heat fluxes derived from COADS from January, 1945 to December, 1989. Also cloud effects to satellite derived data can contribute to the model SST being warmer than TMI-SST. The presence of a roughly 50km data gap along the coastal zone (East African ocean) in the satellite SST (TMI SST) which is attributed to contamination of Satellite radiometer by continental or Island landmasses prevents a direct comparison with the model results near the coast.

The Tanzanian coastal ocean and the adjacent ocean have warm SST of greater than 28^0C in the transition periods to the South West monsoon (May) and to the North East monsoon (November); and at the peak and end of the North East monsoon in January and March respectively. During May, the weak winds along the equator to the north of the model domain (Figure 4.2a) lead to a net heat flux gain (Figure 4.1a) which contributes to warm sea surface temperatures as shown in both model SST and TMI-SST (Figures 4.1 b, c). The region with strong south-easterly winds corresponds to the net heat flux loss which contributes to the cooling SST as shown in figures 4.1b, c. In November, the regions with weak winds get heated by the increased solar radiation in austral summer. Hence, there is a rise in SST in the southwest, north and east of the model domain (Figures 4.2d, 4.1j, k, l). In January and March, the strong winds in the north of the model domain cool the SST which results in a net heat flux gain from the atmosphere. The weak winds over the south of the model domain cause weak evaporation and mixing and hence lead to high SST and a low heat gain is an evident (Figure 4.2) except in east of Madagascar and

south of 10^0S in January. In January, south of 10^0S, there are very weak winds which correspond to the relatively high net heat flux gain which contribute to warming of the SST. During July, the strong south-easterly winds over the southeast of the domain and southerly winds over the southwest of the model domain lead to evaporation which is shown by the net heat flux loss and the cooling SST is evident (Figures 4.2b, 4.1d, e, f). The weak winds correspond to relatively warm SST which can be caused by the net heat flux gain. In September, when the sun is overhead of Tanzania and the South West monsoon ends, the strong south-easterly winds over the southeast of the domain cause the net heat flux loss which cools the SST while the regions with weak winds is dominated by great net heat gain which result in the relatively warm SST (Figures 4.2c, 4.1g, h, i).

The EACC appears to be mainly affected by the reversal of the winds over the Indian Ocean resulting in both spatial and temporal variations in its speeds. There is a strong positive correlation ($r>0.6$ and $p<0.05$) between the EACC and their corresponding meridional wind stresses off the East African coast between 40 and 42^0E. The reversals of the southeast and northwest winds over the north of 12^0S to the equator in both austral winter and summer respectively (Hermes and Reason, 2008; Tomczak and Godfrey, 1994) oppose and support the current respectively. This is shown by the multiple plot axes of the point time series of the EACC speeds and their corresponding meridional wind stresses at 10^0S, 8^0S, 6^0S, 4^0S and 2^0S between 40^0E and 42^0E whereby the correlation coefficient is greater than 0.6 and p-values less than 0.05 at all locations (Figure 4.4). The southward meridional wind stresses during the North East monsoon (December to March) oppose the northward

flowing EACC, and hence it gets weaker than the rest of the year and the weakness decrease northwards (Figures 4.3a, b, c, l and 4.4). The EACC meets with the seasonal southward Somali Current at 1^0S in December, January and March and at 2^0S in February. The minimum speeds of less than 0.9ms^{-1} occur in February as explained by Tomczak et al. (1994) for all locations along the coast of East Africa at approximately 40 to 42^0E. The northward meridional wind stresses along the EACC occur between April and November while during March/April and November they tend to be nearly zero. During the period between April and November, the EACC gets strengthened by those northward meridional wind stresses. As a result, there is an increase in speeds of the EACC with spatial increase northward (Figures 4.3d, e, f, g, h, i, j, k, 4.4, Table 4.1). By this time, the Somali Current flows northwards as an extension of the EACC. The maximum speed of the EACC is apparent in July when the North East monsoon is fully developed with approximate value of 1.65ms^{-1} at 2^0S between 40 and 42^0E. During both transition seasons (April/May and October/November), the EACC is observed to have speeds greater than 1ms^{-1} to the north of 6^0S and the speeds less than 1ms^{-1} occur to the south of 6^0S.

Both speeds of the flow off the southern Tanzanian coast and that to the north of Madagascar appear to increase and decrease simultaneously during October to April and their minimum speeds in both co-occur in November. The speeds of the flow off the southern Tanzanian ocean decrease from April to May and then increase in June while that to the north of Madagascar act in reverse. From June to July, both flow speeds decrease followed by further decrease in August to the north of Madagascar flow. The latter can be associated with strong meridional wind stresses that do not

support the northwest NEMC. The flow off the southern Tanzanian coast attains its maximum speed in August when the South West monsoon is fully developed which supports the EACC. The flow north of Madagascar attains its maximum speed in September when the South West monsoon fades. In general, there is strong positive correlation (about r=0.57 and p=0.05) between the coastal ocean flow off southern Tanzania and that off North Madagascar.

In terms of recommendations, several studies accompanied by the numerical modeling especially coupled ocean-atmosphere models should be conducted in this region so that a greater understanding of the regional dynamics can be deduced. ROMS is an ocean modeling systems and need to be coupled with an atmosphere model(s) to build understanding of the ocean-atmosphere interaction in the region. Inter-annual studies should be done to help understand the effects of ENSO, the Madden-Julian Oscillation (MJO) and IODZM in the western Indian Ocean and on the EACC. The high resolution datasets which are less affected by clouds and continental contamination like Synthetic Aperture Radar (SAR) data are useful for studying the continental shelf ocean dynamics and flow. This will lead improved comparison of model results near the mainland with the satellite data and as a result better understanding of the dynamics and properties of the coastal ocean.

References

Allan, R., Reason, C., Lindesay, J., and Ansell, T., 2003: Protracted ENSO episodes and their impacts in the Indian Ocean Region. *Deep-Sea Research Part II*, **50**, 2331-2347.

Alory, G., Wijffels, S., and Meyers, G., 2007: Observed temperature trends in the Indian Ocean over 1960—1999 and associated mechanisms. *Geophysical Research Letters*, **34**, L02606, doi: 10.1029/2006GL028044.

Alusa, A. L., and Gwange, P. M., 1978: The occurrence of dry spells during the East African long rains. Research report No. 5/78, East African Institute of Meteorology, pp 1-18.

Alusa, A., and Mushi, M., 1973: A study of the onset, duration and cessation of the rains in East Africa. Proceedings of the Fifth Specialist Meeting on Applied Meteorology in East Africa, Nairobi, Kenya, pp 133-140.

Anderson, D. L. T., and Carrington, D. J., 1993: Modeling interannual variability in the Indian Ocean using momentum fluxes from the operational weather analyses of the United Kingdom Meteorological Office and European Centre for Medium Range Weather Forecasts. *Journal of Geophysical Research,* **98,** 12483–12499.

Anderson, D. L. T., Carrington, D. J., Correy, R., and Gordon, C., 1993: The temporal evolution of equatorial currents in the Indian Ocean. Meteorological Office Climate Research Technical Note 23, Bracknell, Berkshire, United Kingdom, 51 pp.

[Available from U.K. Meteorological Office, Bracknell, Berkshire RG12 252, United Kingdom]

Ashok, K., Chan, W. L., Motoi, T., Yamagata, T., 2004: Decadal variability of the Indian Ocean dipole. *Geophysical Research Lett*ers, **31**, L24207, doi: 10.1029/2004GL021345.

Behera, S., and Yamagata, T., 2001: Subtropical SST dipole in the Southern Indian Ocean. *Geophysical Research Letters,* **28(2)**, 327-330.

Bell, B. E., 1972: Marine fisheries. In: Morgan, W. T. W. (ed.) East Africa: its people and resources. Oxford University Press, London, pp 243-254.

Biastoch, A., Krauss, W., 1999: The role of mesoscale eddies in the source regions of the Agulhas Current. *Journal of Physical Oceanography,* ***29*****,** 2303–2317.

Bjerknes, J., 1966: A possible response of the atmospheric Hadley circulation to equatorial anomalies of ocean temperature. *Tellus*, **18**, 820-829.

Bjerknes, J., 1972: Large-scale atmospheric response to the 1964–65 Pacific equatorial warming. *Journal of Physical Oceanography,* ***2*** **(3),** 212–217.

Canuto, V.M., Howard, A., Cheng, Y., Dubovikov, M. S., 2001: Ocean turbulence I: one point closure model. Momentum and heat vertical diffusivities. *Journal of Physical Oceanography*, **31**, 1413-1426.

Chambers, D. P., Tapley, B. D., and Stewart, R.H., 1999: Anomalous warming in the Indian Ocean Coincident with El-Nino. *Journal of Geophysical Research*, **104(C2),** 3035-3047.

Colberg, F., and Reason, C.J.C., 2006: A model study of the Angola Benguela Frontal Zone: Sensitivity to atmospheric forcing. *Geophysical Research Letters*, **33(19)**, L19608.

Cutler, A. N., and Swallow, J. C., 1984: Surface currents of the Indian Ocean. (To 25°S, 100°E). I. O. S. Technical Report 187.

Da Silva, A. M., Young, C.C., Levitus, S., 1994: Atlas of the surface marine data 1994, volume **1**, algorithms and procedures, Technical report, U.S. Department of Commerce, NOAA.

de Ruijter, W. P. M., Brummer, G. -J. A., Drijfhout, S. S., Lutjeharms, J. R. E., Peeters, F., Ridderinkhof, H., van Aken, H., and van Leeuwen, P. J., 2006: Observations of the Inter-Ocean Exchange Around South Africa. *Eos, Transactions, American Geophysical Union*, ***87*(9),** doi: 10.1029/2006EO090002.

Di Lorenzo, E., Miller, A.J., Neilson, D.J., Cornuelle, B.D., Moisan, J.R., 2003: Modeling observed California Current mesoscale eddies and the ecosystem response. *International Journal of Remote Sensing.*

Diaz, H., and Markgraf, V., 2000: El Nino and Southern Oscillation: Multi-scale Variability and global and regional Impacts (Cambridge University Press, London).

Dubi, A. M., 1998: (Manuscript) "Evaluation of extreme wind speeds in relation to the design of coastal structures in Tanzania", *Uhandisi Journal*, Faculty of Engineering, University of Dar es Salaam

Dubi, A. M., 1999: Evaluation of extreme wind speeds in relation to the design of coastal structures in Tanzania. *Uhandisi Journal,* **23(1),** 57–63.

Dubi, A. M., 2000: Coastal erosion. In: Ngusaru, A.S. (Ed). The present state of knowledge of marine science in Tanzania: synthesis report. Tanzania Coastal Management Partnership, Science and Technical Working Group. May 2000.

Dubi, A.M., Frequency and long-term distribution of coastal winds of Tanzania. http://gridnairobi.unep.org/chm/EAFDocuments/Tanzania/Coastal_winds_of_Tanzania.pdf.

Düing, W., Schott, F., 1978: Measurements in the source region of the Somali current during monsoon reversal. *Journal of Physical Oceanography,* **8,** 278-289.

E.A.M.D (East African Meteorological Department)., 1963a: Climatic seasons of East Africa. East African meteorological Departmental Report No.8, 4pp.

E.A.M.D. (East African Meteorological Department)., 1963b: The weather of East Africa, East African meteorological Department. Pamphlet series No.7, 13pp.

Francis, J., Mahongo, S., and Semesi, A., 2000: The coastal environment. In: Eastern Africa atlas of coastal resources of Tanzania. UNEP. Nairobi, Kenya.

Gadgil, S., 2003: The Indian monsoon and its variability. *Annual Reviews of Earth and Planetary Sciences, **31,*** 429–67.

Galperin, B., Kantha, L. H., Hassid, S., and Rosati, A., 1988: A quasi-equilibrium turbulent energy model for geophysical flows. *Journal of Atmospheric Science,* **45**, 55-62.

Godfrey, J.S., and co-authors., 1995: The Role of the Indian Ocean in the Global Climate System: Recommendations Regarding the Global Ocean Observing System. *Report of the Ocean Observing System Development Panel, Texas A&M University, College Station, Tex, USA.89pp.*

Gordon, G. L., and McClean, J. L., 1999: Thermohaline stratification of the Indonesian Seas: model and observations. *Journal of Physical Oceanography*, **29**, 198–216.

Grant, R.B., 1996: The Oceans and Climate. Cambridge University Press, 1996.

Griffiths, J., 1959: The variability of annual rainfall in East Africa. *Bulletin of America Society*, **44,** 361-362.

Hacker, P., Firing, E., Hummon, J., Gordon, A., and Kindl, J. C., 1998: Bay of Bengal currents along the northeast monsoon. *Geophysical Research Letters*, **25**, 2769–2772.

Haidvogel, D. B., Arango, H. G., Hedstrom, K., Beckmann, A., Malanotte-Rizzoli, P., and Shchepetkin, A. F., 2000: Model evaluation experiments in the North

Atlantic Basin: Simulations in nonlinear terrain-following coordinates. *Dynamics of Atmospheres and Oceans*, **32**, 239-281.

Halley, E., 1686: An historical account of the trade winds and monsoons observable in the seas between and near the tropical with an attempt to assign a physical cause of the said winds. *Philosophical Transactions of the Royal Society*, London, **16**,153-68.

Han, W., McCreary, J. P. Jr., Anderson, D. L. T., and Mariano, A. J., 1999: On the dynamics of the eastward surface jets in the equatorial Indian Ocean. *Journal of Physical Oceanography,* **29**, 2191–2209.

Hermes, J.C., and Reason, C.J., 2008: Annual cycle of the South Indian Ocean (Seychelles-Chagos) thermocline ridge in a regional ocean model. *Journal of Geophysical Research,* **113**, C04035, doi: 10.1029/2007JC004363.

Hickey, B., 1975: The relationship between Fluctuations in Sea Level, Wind Stress and Sea Surface Temperature in Equatorial Pacific. *Journal of Physical Oceanography,* **5**, 460-475.

Jensen, T. G., 1991: Modeling the seasonal undercurrents in the Somali Current system. *Journal of Geophysical Research*, **96**, 22151–22167.

Jensen, T. G., 1993: Equatorial variability and resonance in a wind-driven Indian Ocean Model. *Journal of Geophysical Research*, **98**, 22533–22552.

Julius, A., 2005: Monitoring programme for resource condition, environmental and biological parameters for Mnazi Bay Ruvuma estuary marine park (MBREMP)

Tanzania, Final Project, Fisheries Training Programme, The United Nations University, Iceland.

Kabanda, T. A., 1995: Seasonal and Intra-seasonal dynamics and precursors of rainfall over northern Tanzania. MSc. Thesis, University of Cape Town, South Africa.

Kantha, L. H., and Clayson, C. A., 1994: An improved mixed layer model for geophysical applications. *Journal of Geophysical Res*earch, **99**, 25235-25266.

Kijazi, A., and Reason, C., 2005: Relationships between Intraseasonal Rainfall Variability of Coastal Tanzania. *Journal of Theoretical and Applied Climatology,* **82**, 153-176.

Knox, R., 1976: On a long series of measurements of Indian Ocean equatorial currents near Addu Atoll. *Deep-Sea Research*, **23**, 211–221.

Krishnamurti, T.N., 1971a: Observational study of the tropical upper tropospheric motion field during the northern hemisphere summer. *Journal of Applied Meteorology,* 1**0**, 1066-1096.

Krishnamurti, T.N., 1971b: Tropical east-west circulation during the northern summer. *Journal of Atmospheric Science*, **28**, 1342-1347.

Krishnamurti, T., 1996: Monsoons. *Encyclopedia of Climate and Weather*, **2,** 512-515. Oxford University Press, New York.

Kumar, D., 2001: Monthly Mean Sea Level Variations at Cochin, Southwest of India. *International Journal of Ecology and Environmental Science,* **27**, 209-214.

Large, W.G., McWilliams, J.C., and Doney, S.C., 1994: Oceanic vertical mixing: a review and a model with a non-local boundary layer parameterization. *Reviews of Geophysics*, **32**, 363-403.

Leetmaa, A., and Stommel, H., 1980: Equatorial current observations in the western Indian Ocean during 1975 and 1976. *Journal of Physical Oceanography*, **10**, 258–269.

Leetmaa, A., Quadfasel, D. R., Wilson, D., 1982: Development of the flow field during the onset of the Somali current, 1979. *Journal of Physical Oceanogr*aphy, **12**, 1325-1342.

Levitus, S., and Boyer, T., 1994: World Ocean Atlas, Vol. **4**: Temperature, NOAA Atlas NESDIS 4, NOAA, Washington, DC, 117pp, 1994b.

Loschnigg, J., Meehl, G. A., Arblaster, J. M., Compo, G. P., and Webster, P.J., 2003: The Asian monsoon, the tropospheric biennial oscillation, and the Indian Ocean Dipole in the NCAR CSM. *Journal of Climate*, **16**, 1617-1642.

Lutjeharms, J. R. E., Wedepohl, P. M., and Meeuwis, J. M., 2000: On the surface drift of the East Madagascar and Mozambique currents. *South African Journal of Science,* **96**, 141– 147.

Mahongo, S.B., 1999: The Tanzanian Sea Level Network. Draft report submitted to IOC, 16pp.

Maltrud, M. E., Semtner, A. J., and Malone, R. C., 1998: Global eddy-resolving ocean simulation driven by 1985–1995 atmospheric winds. *Journal of Geophysical Research*, **103**, 30825–30853.

Marchesiello, P., McWilliams, J. C., and Shchepetkin, A., 2003: Equilibrium structure and dynamics of the California Current System. *Journal of Physical Oceanography,* **33**, 753-783.

Mayorga-Adame, G.C., 2007: Ocean Circulation of the Zanzibar Channel: A modeling Approach. Theiss Research, La Jolla, California, USA.

McClanahan, T. R., 1988: Seasonality in East Africa's coastal waters. *Marine Ecology-Progress Series*, **44**, 191-199.

McPhaden, M. J., Meyers, G., Ando, K., Masumoto, Y., Murty, V. S. N., Ravichandran, M., Syamsudin, F., Vialard, J., Yu, L., Yul, W., 2008: RAMA: The Research Moored Array for African-Asian-Australian Monsoon Analysis and Prediction. Submitted to the *Bulletin of the American Meteorological Society,* USA, 53 pp.

Mellor, G. L., and Yamada, T., 1982: Development of a turbulence closure model for geophysical fluid problems. *Reviews of Geophysical and Space Physics,* **20**, 851-875.

Mhita, M.S., and Nassib, I. R., 1987: The onset and end of rain in Tanzania. Proc. 1st Tech. Conference. Meteor. Res. Eastern and Southern Africa, Nairobi, pp 101-115.

Moore, A. M., Arango, H. G., Miller, A. J., Cornuelle, B. D., Di Lorenzo, E. and Neilson, D. J., 2004: A Comprehensive Ocean Prediction and Analysis System Based on the Tangent Linear and Adjoint Components of a Regional Ocean Model. *Ocean Modelling*, **7**, 227-258.

Morrow, R., and Birol, F., 1998: Variability in the southeast Indian Ocean from altimetry: Forcing mechanism for the Leeuwin Current. *Journal of Geophysical Research,* **103**, 18529–18544.

Mpeta, E. J., 1997: Intra-seasonal convection dynamics over southwest and northeast Tanzania: An observational study. MSc. Thesis, University of Cape Town, South Africa.

Mwandosya, M., Nyenzi, B.S., and Luhanga, M. L., 1998: The Assessment of Vulnerability and Adaptation to Climate Change Impacts in Tanzania. The Centre for Energy, Environment, Science and Technology, Dar es Salaam, 235 pp.

Newell, B.S., 1957: A preliminary survey of the hydrography of the British East African Coastal waters. Fishery Publications No. 9. Her Majesty's Stationery Office, London, 21 pp.

Newell, B.S., 1959: The hydrography of British East African coastal waters. II. *Fishery Publications*, London, **12**, 1-18.

Ngwali, M.K., 2006: Sea Level and Climate Variability at Zanzibar. MSc. Thesis, University of Cape Town, South Africa.

Nyandwi, N., and Dubi, A., 2001: Episodic atmospheric changes and their impact on the hydrography of coastal waters in Tanzania. *Climate Research,* **18**, 157 – 162.

Nyenzi, B. S., 1988: Mechanism of the East African variability, PhD Thesis, Florida state University, 184 pp.

O'Brien, J. J., and Hurlburt, H. E., 1974: An equatorial jet in the Indian Ocean theory. *Science,* **184**, 1075–1077.

Ogallo, L.J., 1989: The spatial and temporal patterns of the East African seasonal rainfall derived from principle component analysis, Royal Meteorological Society.

Parker, S., 1992: Sea level as an indicator of climate and global change. *Marine Technology Society Journal, Volume* **25**, No. 4.

Peliz, A., Dubert, J., Haidvogel, D. B., and Le Cann, B., 2003: Generation and unstable evolution of a density-driven Eastern Poleward Current: The Iberian Poleward Current. *Journal of Geophysical Research*, **108(C8)**, 3268, doi: 10.1029/2002JC001443.

Penven, P., Debreu, L., Marchesiello, P., McWilliams, J. C., 2006: Application of the ROMS embedding procedure for the Central California Upwelling System. *Ocean Modelling,* **12**, 157-187.

Penven, P., Echevin, V., Pasapera, J., Coals, F., Tam, J., 2005: Average circulation, seasonal cycle and mesoscale dynamics of the Peru Current System: A modelling approach. *Journal of Geophysical Res*earch, **110**, C10021, doi: 10.1029/2005JC002945.

Penven, P., Roy, C., Brundrit, G. B., Colin de Verdière, A., Fréon, P., Johnson, A. S., Lutjeharms, J. R. E., and Shillington, F. A., 2001: A regional hydrodynamic model of the Southern Benguela. *South African Journal of Science*, **97**, 472-476.

Penven, P., 2000: A numerical study of the Southern Benguela Circulation with an application to fish recruitment. PhD thesis, Universite de Bretagne Occidentale, Brest.

Penven, P., Tan, T., 2007: ROMSTOOLS User's Guide. Institut de Recherche pour de Dèveloppement (IRD), 213 rue Lafayette, Paris, France.

Philander, S.G.H., 1999: A review of tropical ocean-atmosphere interactions. *Tellus,* **51A-B (1)**, 71-90.

Philander, S.G.H., 1990: El Nino, La Nina, and the Southern Oscillation. *Academic Press,* London, 289 pp.

Philander, S.G.H., 1998: *Is the Temperature Rising: The Uncertain Science of Global Warming*, Princeton, NJ: Princeton University Press, 240 pp.

Phinn, S., and Hastings, P., 1992: Southern Oscillation Influences on the Wave Climate of South-East Australia. *Journal of Coastal Research,* **8 (3),** 579-592.

Picaut J., Masia, F., and Penhoat, Y., 1997: An advective-reflective conceptual model for the oscillatory nature of the ENSO. *Science,* **277 (5326),** 663–666.

Pickard, G. L., and Emery, W. J., 1990: Descriptive Physical Oceanography. 5th , Pergamon Press, Oxford, UK.

Quadfasel, D., and Schott, F., 1982: Water mass distribution at intermediate layers off the Somali coast during the onset of the southwest monsoon, 1979. *Journal of Physical Oceanography*, **12**, 1358–1372.

Rao, G.L.V., and Ram, S. P., 2005: Upper ocean physical processes in the Tropical Indian Ocean, National institute of Oceanography, Goa, India, 68 pp.

Rao, R.R., and Sivakumar, R., 2000: Seasonal variability of near-surface thermal structure and heat budget of the mixed layer of the tropical India n Ocean from a new global ocean temperature climatology. *Journal of Geophysical Res*earch, **105(C1),** 995-1015.

Rao, R.R; Molinari, R.L., and Festa, J.F., 1989: Evolution of the climatological near-surface thermal structure of the tropical Indian Ocean. 1. Description of mean monthly mixed-layer depth, and sea surface temperature, surface current, and surface meteorological fields. *Journal of Geophysical Research,* **94**, 10801-10815.

Reason, C., Allan, R., Lindesay, J., and Ansell, T., 2000: ENSO and Climatic Signals across the Indian Ocean basin in the global context: Part 1, Interannual Composite Patterns. *International Journal of Climatology,* **20**, 1285-1327.

Reppin, J., Schott, F. A., Fischer, J., and Quadfasel, D., 1999: Equatorial currents and transports in the upper central Indian Ocean: annual cycle and interannual variability. *Journal of Geophysical Research*, **104**, 15495–15514.

Ropelewski, C. F., and Halpert, M. S., 1987: Global and regional scale precipitation patterns associated with the El Niño / Southern Oscillation (ENSO). *Monthly Weather Review*, **115**, 1606-1626.

Ruby, J., and Sete, C., 2002: Sea Level Variation for the Coast of Mozambique. (Africa-America GLOSS news-2002).

Ruitenbeen, J., Hewawasan, I., and Ngoile, M., 2005: *Sustaining the marine environment in mainland Tanzania and Zanzibar*. (eds). Blue print 2050. The World Bank. Washington, DC.

Saji, N. H., Goswami, B. N., Vinayachandran, P. N., Yamagata, T., 1999: A dipole mode in the tropical Indian Ocean. *Nature,* **401,** 360-363.

Saji, N.H., and Yamagata, T., 2003: Structure of SST and Surface Wind Variability during Indian Ocean Dipole Mode Events: COADS observations. *Journal of Climate*, **16**, 2735-2751.

Schott, F., and McCreary, J.P., 2001: The monsoon circulation of the Indian Ocean. *Progress in Oceanography*, **51**, 1-123.

Schott, F. A., Dengler, M., Schoenefeldt, R., 2002: The shallow overturning circulation of the Indian Ocean. *Progress in Oceanography*, **53**, 57-103.

Schott, F. A., Xie, S. P., and McCreary, J. P., 2008: Indian Ocean circulation and climate variability. *Reviews of Geophysics,* submitted.

Schott, F., Swallow, J. C., and Fieux, M., 1990: The Somali Current at the equator: annual cycle of currents and transports in the upper 1000 m and connection to neighboring latitudes. *Deep-Sea Research*, **37**, 1825–1848.

Shaghude, Y.W., 2003: Coastal impacts of water abstraction and impoundment in Africa: The case of Rufiji River. Framework of the African River Catchments (AfriCat). Electronic version, December 2005. (http://iodeweb1.vliz.be/odin/bitstream/1834/187/1/coastal.pdf)

Shchepetkin, A., and McWilliams, J., 2003: A method for computing horizontal pressure-gradient force in an ocean model with a non-aligned vertical coordinate. *Journal of Geophysical Research,* 1**08**, 35.1-35.34.

Shchepetkin, A., and McWilliams, J., 2005: The Regional Oceanic Modelling system (ROMS): A split-explicit, free-surface, topography following coordinate oceanic model. *Ocean modelling*, **9,** 347-404.

Shenoi, S. S. C., Saji, P. K., and Almeida, A. M., 1999: Near-surface circulation and kinetic energy in the tropical Indian Ocean derived from Lagrangian drifters. *Journal of Marine Research*, **57**, 885–907.

Singh, O., Khan T., Aktar, F., and Sarker, M., 2001: Recent Sea Level and Sea Surface Temperature Changes along the Maldives Coast. *Marine Geodesy*, **24,** 209-218.

Singh, O., 2002: Spatial Variation of Sea Level Trend along the Bangladesh Coast. *Marine Geodesy*, **25**, 205-212.

Smith, S.D., 1988: Coefficients for sea surface wind stress, heat flux, and wind profiles as a function of wind speed and temperature. *Journal of Geophysical Research,* **93,** 15467-15472.

Smith, S. L., Codispoti, L. A., 1980: Southwest monsoon of 1979: chemical and biological response of Somali coastal waters. *Science,* **209**, 597-600.

Song, Y., and Haidvogel, D.B., 1994: A semi-implicit ocean circulation model using a generalized topography-following coordinate system. *Journal of Computational Physics*, **115 (1),** 228-244.

Stewart, R.H., 2007: Introduction to Physical Oceanography. Online version.

Styles, R., and Glenn, S. M., 2000: Modelling stratified wave and current bottom boundary layers in the continental shelf. *Journal of Geophysical Research,***105**, 24119- 24139.

Swallow, J., 1967: The equatorial undercurrent in the western Indian Ocean in 1964. *Studies in Tropical Oceanography*, **5**, 15–36.

Swallow, J. C., Fieux, M., and Schott, F., 1988: The boundary currents east and north of Madagascar, Part I: Geostrophic currents and transports. *Journal of Geophysical Research*, **93**, 4951–4962.

Swallow, J. C., Schott, F., and Fieux, M., 1991: Structure and transport of the East African Coastal Current. *Journal of Geophysical Research*, ***96***, 22254–22267.

Taft, B. A., 1967: Equatorial undercurrent of the Indian Ocean, 1963. *Studies in Tropical Oceanography*, **40**, 3–14.

Takayabu, Y.N., Iguchi, T., Kachi, M., Shibata, A., and Kanzawa, H., 1999: Abrupt termination of the 1997-98 El Nino in response to a Madden-Julian oscillation. *Nature*, **402**, 279-282.

Tomczak, M., and Godfrey, J. S., 1994: Regional Oceanography, An introduction. Pergamon, Oxford, UK.

Umlauf, L., Burchard, H., 2003: A generic length-scale equation for geophysical turbulence models. *Journal of Marine Res*earch, **61**, 235-265.

UNEP., 1985: Implications of climate change in the East African coastal region. UNEP Regional Seas Reports and Studies Number 149.

Warner, J. C., Sherwood, C. R., Arango, H. G., and Signell, R. P., 2005: Performance of four Turbulence Closure Methods Implemented using a Generic Length Scale Method. *Ocean Modelling*, **8**, 81-113.

Warren, B., Stommel, H., Swallow, J .C., 1966: Water masses and patterns of flow in the Somali Basin during the southwest monsoon of 1964. *Deep Sea Res*earch, **13**, 825-860.

Warren, J. A., 1966: Medieval Arab references to the seasonally reversing currents of the North Indian Ocean. *Deep Sea Res*earch, **13**, 167-171.

Webster, P. J., 1987: The elementary monsoon. In Monsoons, ed. JS Fein, PL Stephens, pp. 3–32. New York.

Webster, P. J., Moore, A., Loschnigg, J., and Leben, R., 1999: Coupled ocean-atmosphere dynamics in the Indian Ocean during 1997–98. *Nature*, **401**, 356–360.

Wilkin, J. L., Arango, H. G., Haidvogel, D. B., Lichtenwalner, C.S., Durski, S. M., and Hedstorm, K. S., 2005: A regional Ocean Modeling System for the Long-term Ecosytem Observatory. *Journal of Geophysical Res*earch, **110**, C06S91, doi: 10.1029/2003JC002218.

Wyrtki, K., 1973: An equatorial jet in the Indian Ocean. *Science*, **181**, 262–264.

Xie, S.P., Annamalai, H., Schott, F. A., and McCreary, J. P., 2002: Structure and Mechanisms of South Indian Ocean Climate Variability. *Journal of Climate*, **15**, 864–878.

Yamagata, T., Behera, S.K., Luo, J.J., Masson, S., Jury, M.R., and Rao, S.A., 2004: Coupled Ocean-Atmosphere variability in the Tropical Indian Ocean. *Earth's climate*, **147**, 1029/147GM12.

Yang, J., Liu, Q., Xie, S.P., Liu, Z., and Wu, L., 2007: Impact of the Indian Ocean SST basin mode on the Asian summer monsoon. *Geophysical Research Lett*ers, **34**, L02708, doi: 10.1029/2006GL028571.

Yokoi, T., Tozuka, T., and Yamagata, T., 2008: Seasonal variation of the Seychelles Dome. *Journal of Climate*, in press.

Yu, W., Xiang, B., Liu, L., and Liu, N., 2005: Understanding the origins of interannual thermocline variations in the tropical Indian Ocean. *Geophysical Research Lett*ers, **32**, L24706, doi: 10.1029/2005GL024327.

Yu, Y., Mechoso, C., McWilliams, J., and Arakawa, A., 2002: Impacts of the Indian Ocean on the ENSO cycle. *Geophysical Research letters*, **29(8)**, L1204, 10.1029/2001GL014098.